# The Promise of Metal-Halide-Perovskite Solar Photovoltaics: A Brief Review

Nitin P. Padture \*

School of Engineering, Brown University, Providence, RI 02912, USA;
nitin\_padture@brown.edu
\* Corresponding author

ORCID: 0000-0001-6622-8559

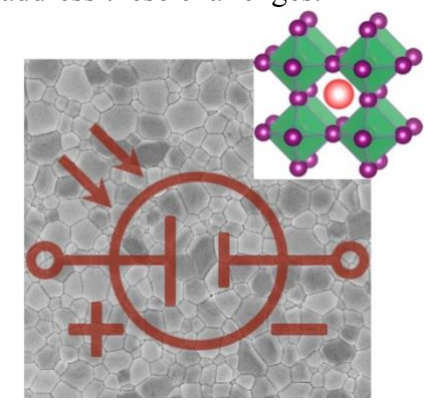
Invited Review Article for the 50<sup>th</sup> Anniversary Issue of the MRS Bulletin (2023)

Manuscript No. MRSB-D-23-00118

### Abstract

Solar photovoltaics (PVs) based on metal-halide perovskites (MHPs) have taken the renewable-energy world by storm. The excitement stems from the promise of a high-efficiency, low-cost, and low 'carbon-footprint' new PV technology. Here, a brief overview of the important topics pertaining to MHPs, perovskite solar cells (PSCs), and perovskite solar modules (PSMs) is presented. The topics include: (i) PSC architectures; (ii) MHPs; (iii) synthesis and processing of MHP thin films; (iv) MHP thin-film microstructures; (v) PSC functional layers; (vi) interfacial engineering in PSCs; (vii) PSC performance; (viii) PSC stability; (ix) PSMs; (x) lead toxicity; and (xi) mechanical behavior and reliability. The significant challenges in the path towards commercialization of this burgeoning PV technology are also highlighted. Chief among them are scalability, stability, reliability, and safety, while achieving high efficiency, low cost, and low 'carbon-footprint.' The promise of this new PV technology, and the fascinating underlying science, make it a worthwhile endeavor to address these challenges.

# **Graphical Abstract**



**Keywords:** perovskites; thin films; solar cells; photovoltaics

### Introduction

Renewable electricity from solar photovoltaics (PVs), combined with low-cost large-scale storage, will play a key role in decarbonizing and expanding the global power sector. For example, the global deployment of PVs is targeted at ~75 TW installed capacity by 2050, from the current (2022) ~1 TW.<sup>[1]</sup> This is expected to contribute towards limiting global warming to 1.5 °C above the pre-industrial age stated in the COP-21 2015 Paris agreement, thereby avoiding the dire consequences of global climate change. While the ~75 TW target may seem aggressive, the fact remains that PVs are likely to dominate the global power sector for achieving and maintaining a net-zero-carbon future. Currently used PV technologies are efficient, reliable, and relatively cheap, but there is, and always will be, demand for new PV technologies that are more efficient, reliable, cost-effective, and importantly, have a lower 'carbon-footprint.'

In this context, perovskite solar cells (PSCs) based on metal-halide-perovskite (MHP) thinfilm light-absorbers hold great promise. [2-4] This is because PSCs can be made at near-room temperatures, employing potentially scalable processes, and they use very small amounts of earthabundant materials. Thus, the estimated energy-payback time and greenhouse-gas emission for PSCs can be as low as  $\sim 0.09$  years and  $\sim 13.35$  g CO<sub>2</sub> eq./KWh, respectively, relative to  $\sim 1.3$  years and ~29.67 g CO<sub>2</sub> eq./KWh for comparable state-of-art Si PVs.<sup>[5]</sup> The excitement about PSCs worldwide is driven in part by their power conversion efficiency (PCE), which, at least at the lab scale, rivals that of Si PVs; Fig. 1 plots the progression of certified record PCEs of select PV technologies in recent years from the National Renewable Energy Laboratory (NREL) Best Research-Cell Efficiency Chart. [6] Note the strikingly rapid progress of single-junction PSCs, from 3.8% since their invention in 2009 by Miyasaka and coworkers, [7] to the current certified record PCE of 26.0% (ISCAS) in 2023. [6] In addition to utility-scale and rooftop PVs, PSCs offer new functionalities, owing to some unique attributes they possess, for potential use in: tandem PVs; building-integrated PVs; light-weight flexible PVs for consumer applications (backpacks, tents, portable power source, drones, etc.); indoor PVs; and PVs for space application. Not surprisingly, PSCs are one of the most widely researched topics, with a staggering 30,000+ journal papers published in the area since 2009 (Source: Clarivate Web of Science). Materials Research Society (MRS) has been at the forefront in convening PSC researchers by hosting numerous well-attended symposia, starting with the 2013 MRS Fall Meeting in Boston.

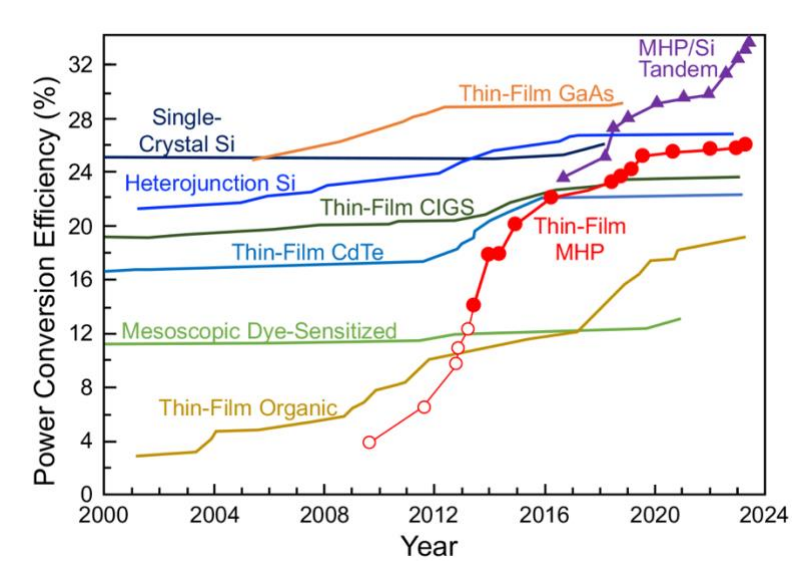


**Figure 1.** Recent progression of certified record PCEs (lab-scale solar cells) of select single-junction PV technologies and MHP/Si tandem PVs from NREL Best Research Cell Efficiency Chart. Light red circles are not certified PCEs. Adapted from ref.<sup>[6]</sup>

# Perovskite solar cell (PSC) architectures

To understand the evolution of PSC architectures one must look to the early history of PSC development, which traces its origins to the dye-sensitized solar cell (DSSC) (also called the 'Grätzel cell').[8] The first PSC was a DSSC comprising mesoscopic TiO<sub>2</sub> scaffold decorated with organic-inorganic MHP nanoparticles as the dye, reporting a PCE of 3.8% in 2009.<sup>[7]</sup> Park, Grätzel, and coworkers replaced the liquid electrolyte commonly used in DSSCs with a solid in 2012 to achieve 9.7% PCE. [9] Around the same time, Kanatzidis, Chang, and coworkers replaced the liquid electrolyte with an inorganic MHP, but used a traditional DSSC dye, to achieve 10.2% PCE; [10] it was implied that the MHP was also contributing to light-absorption. Also in 2012, an insulating mesoscopic scaffold (Al<sub>2</sub>O<sub>3</sub>), coated with MHP, was used by Snaith and coworkers to achieve a PCE of 10.9%.[11] In 2013, Seok, Grätzel, and coworkers introduced the bi-continuous PSC that used a mesoscopic TiO<sub>2</sub> scaffold with interpenetrating MHP, instead of surface decoration, to achieve 12% PCE.<sup>[12]</sup> In the same year, inspired by organic photovoltaics (OPVs), Snaith and coworkers demonstrated 6.4% efficiency 'inverted' (p-i-n) planar PSCs without the mesoporous scaffold.[13] By removing the need for higher temperatures (400-500 °C) to sinter the oxide mesoscopic scaffold, these planar PSCs could be deposited on flexible plastic substrates.<sup>[13]</sup> In 2014, Snaith and coworkers demonstrated 'regular' (n-i-p) planar PSCs on glass substrates with

11.4% PCE.<sup>[14]</sup> In the same year, Seok and coworkers added a planar MHP capping layer to bicontinuous mesoscopic *n-i-p* PSCs to achieve 16.2% PCE.<sup>[15]</sup> This hybrid architecture, which is almost exclusively *n-i-p*, together with *n-i-p* planar and *p-i-n* planar, are the three most commonly researched basic single-junction PSC architectures today, and are depicted schematically in Figs. 2a, 2b, and 2c, respectively. The highest PCE PSCs are *n-i-p*, but generally *p-i-n* PSCs are more stable and are better suited for tandem PV application. The basic operation of PSCs entails strong absorption of sunlight by the MHP thin film, creation of loosely bound electron-hole pairs, and the extraction of separated electrons and holes by the electrode layers through selective *n*-type electron-transport layer (ETL) and *p*-type hole-transport layer (HTL), respectively, on either side of the MHP.<sup>[16]</sup> MHPs have remarkable charge transport properties, where the carrier diffusion lengths and lifetimes are surprisingly long, while the mobilities are modest.<sup>[16-18]</sup>

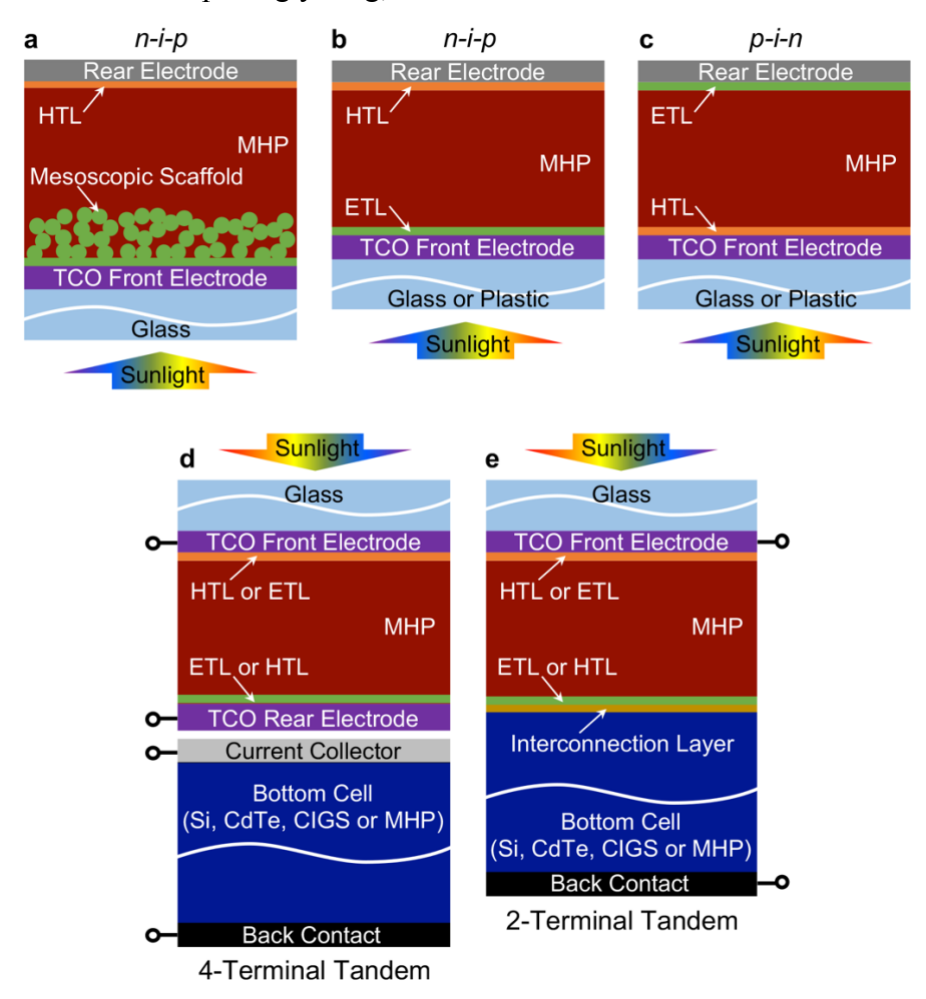


**Figure 2.** Schematic illustrations of popular single-junction PSC and tandem PV architectures: (a) *n-i-p* bicontinuous mesoscopic with capping layer, (b) *n-i-p* planar, (c) *p-i-n* planar, (d) four-terminal tandem, and (e) two-terminal tandem. Not to scale.

There are several variations of the architectures shown in Figs. 2a-2c, and there is a wide variety of materials that are used in the PSC multi-layer stack: electrodes, ETL, HTL, and MHP thin film. [19] The MHP thin films themselves can have a variety of base compositions, which are typically enhanced by doping, alloying, and additives incorporation. Also, the MHP thin films can have a variety of microstructures and grain-boundary characteristics. Furthermore, additional thin layers made of various materials are incorporated at the MHP/ETL and MHP/HTL interfaces. [19] Since the entire PSC multi-layer stack above the transparent-conducting oxide (TCO) front electrode in Fig. 2 is typically <1 μm thick, PSCs can be made flexible and lightweight when deposited on thin (100-200 μm) plastic substrates (*e.g.* polyethylene terephthalate (PET) or polyethylene naphthalate (PEN)), instead of rigid glass (1-3 mm) or Si (150-300 μm), using low-temperature processes. [20, 21]

Since MHP bandgaps are highly tunable *via* compositional engineering, wide-bandgap PSCs can be used as the 'top' solar cell in conjunction with narrow-bandgap 'bottom' solar cells based on Si, CdTe, copper indium gallium selenide (CIGS), or MHPs, to create tandem PVs (double-junction).<sup>[22]</sup> Figures 2d and 2e depict generic tandem PV four-terminal and two-terminal architectures, respectively. Here the 'top' PSC is designed to absorb the complementary shorter-wavelength part of the solar spectrum that the 'bottom' solar cell does not absorb, to reach PCE levels that cannot be achieved in single-junction PVs constrained by the Shockley-Queisser (S-Q) limit. While in four-terminal tandem PVs the two cells are physically stacked on top of each other, in two-terminal tandem PVs the two cells are bonded *via* an interconnection layer that helps match the current outputs of the two cells. Tremendous progress has been made in tandem PV, and the current certified record PCE of PSC/Si tandem PVs stands at 33.7% (KAUST) in 2023 (Fig. 1).<sup>[6]</sup> PSCs in conjunction with OPVs are also being considered, where the order of the cells is reversed.<sup>[22]</sup>

# **Metal-halide perovskites (MHPs)**

At the heart of PSCs is the direct-bandgap semiconductor MHP thin film, which happens to have excellent light-absorption properties. Figure 3a shows higher optical absorption coefficients in a prototypical MHP, methylammonium lead triiodide (CH<sub>3</sub>NH<sub>3</sub>PbI<sub>3</sub> or MAPbI<sub>3</sub>), relative to GaAs and Si, and it also has a sharp absorption edge.<sup>[16, 23]</sup> This is remarkable considering that MHP thin films are quite defective because they are made using less-exacting,

near-room-temperature methods, such as solution-processing ('benches-and-beakers' approach). The phenomenal success of PSCs is also attributed to the unique defect-tolerance properties of MHP materials, where energetically favorable point defects in MHPs occupy 'shallow' states near the conduction band minimum (CBM) or valance band maximum (VBM); Fig. 3b shows calculated energy levels and formation energies of possible point defects in MAPbI<sub>3</sub>.<sup>[24]</sup> Although it is now recognized that these defects may adversely affect other MHP properties such as stability. Additional beneficial effects in MHPs deemed responsible for the unexpectedly superior performance of PSCs include: large-polarons, <sup>[25, 26]</sup> ferroelectricity, <sup>[27-29]</sup> and photon-recycling. <sup>[30, 31]</sup>

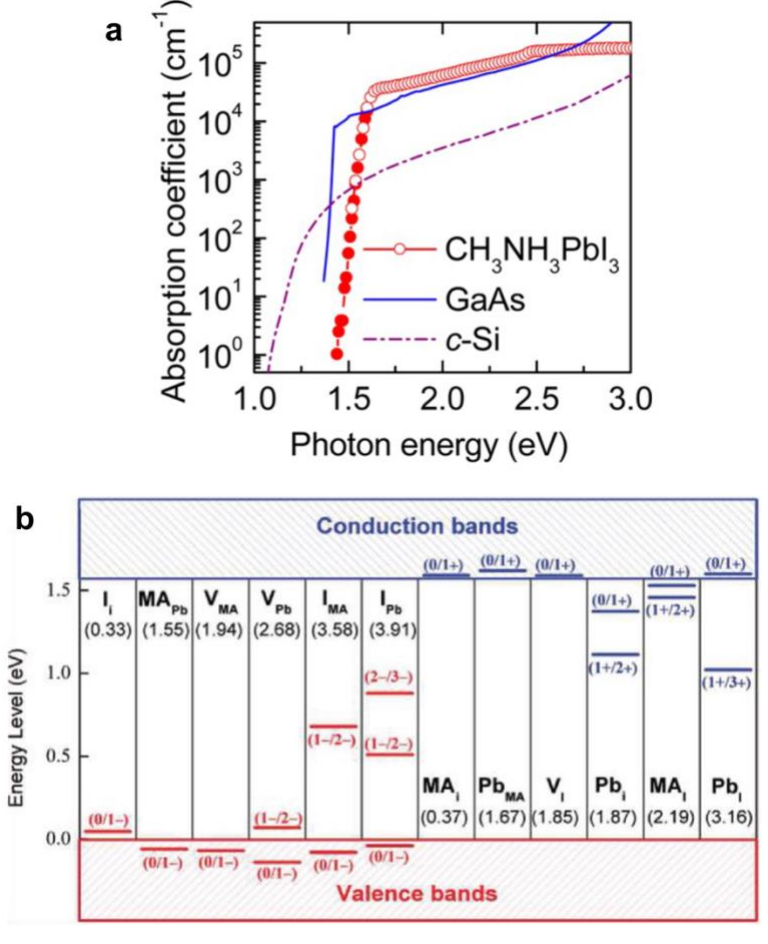


**Figure 3.** (a) Optical absorption coefficients of MAPbI<sub>3</sub> MHP, GaAs, and Si.<sup>[23]</sup> (b) Point defects and their corresponding energy levels and formation energies in MAPbI<sub>3</sub> MHP.<sup>[24]</sup> Reproduced with permission.

The generic 3D perovskite (AMX<sub>3</sub>) structure is depicted in Fig. 4a, where typically monovalent A<sup>1+</sup> is Cs<sup>1+</sup>, MA<sup>1+</sup> (methylammonium CH<sub>3</sub>NH<sub>3</sub><sup>1+</sup>), or FA<sup>1+</sup> (formamidinium

HC(NH<sub>2</sub>)<sub>2</sub><sup>1+</sup>); divalent M<sup>2+</sup> is Pb<sup>2+</sup>, Sn<sup>2+</sup>, or Ge<sup>2+</sup>; and X<sup>1-</sup> is Cl<sup>1-</sup>, Br<sup>1-</sup>, or I<sup>1-</sup>.[32,33] The organic A<sup>1+</sup> cation is weakly bonded and it rotates inside the 'cage.' The stability of the perovskite structure is empirically determined by the Goldschmidt tolerance (0.8<t<1) and octahedral (0.4< $\mu$ <0.9) factors,  $t = (r_A + r_X)/\{\sqrt{2}(r_M + r_X)\}$  and  $\mu = (r_M/r_X)$ , respectively, with r being the corresponding effective ionic radii.[34] This limits the choice of cations and anions, but allows for extensive substitutional solid-solution alloying at all three sublattice sites (A, M, X) to achieve structural stability and the desired optoelectronic properties in so-called 'mixed' MHPs. There are other derivative 3D structures (double perovskites) with general formulae A<sub>2</sub>M(I)M(III)X<sub>6</sub> and A<sub>2</sub>M(IV)X<sub>6</sub>, where typically A<sup>1+</sup> is K<sup>1+</sup>, Rb<sup>1+</sup>, Cs<sup>1+</sup>, In<sup>1+</sup>, MA<sup>1+</sup>, or FA<sup>1+</sup>; M(I)<sup>1+</sup> is Ag<sup>1+</sup>, Cu<sup>1+</sup>, Tl<sup>1+</sup>, or In<sup>1+</sup>; M(III)<sup>3+</sup> is Bi<sup>3+</sup> or Sb<sup>3+</sup>; M(IV)<sup>4+</sup> is Ti<sup>4+</sup>; and X<sup>1-</sup> is F<sup>1-</sup>, Cl<sup>1-</sup>, Br<sup>1-</sup>, or I<sup>1-</sup>.[32]

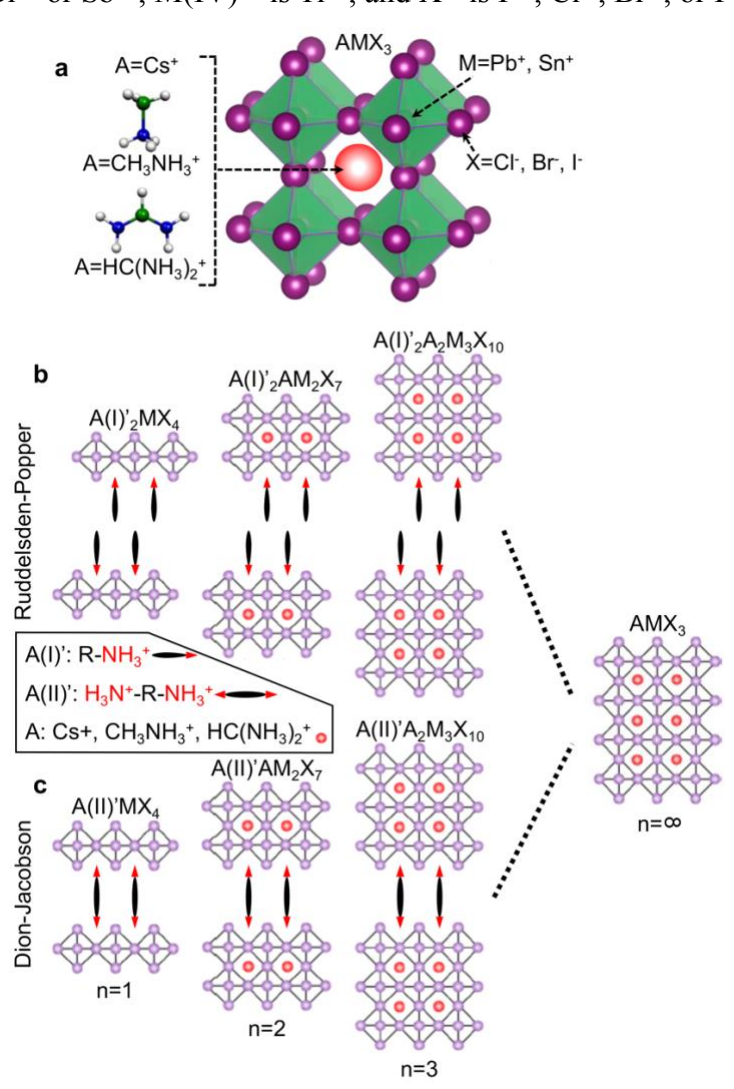


**Figure 4.** Schematic illustrations of generic crystal structures of MHP phases: (a) 3D AMX<sub>3</sub>, (b) LD Ruddlesden-Popper, and (c) LD Dion-Jacobson. Not to scale.

Low-dimensional (LD) layered analogs of 3D MHPs are possible, and they offer vast flexibility in terms of composition and dimensionality to tune the optoelectronic properties. [32, 35] These structures typically entail LD layers of corner-sharing metal-halide octahedra separated by large A' organic cation 'spacers,' which can be monovalent or divalent resulting in A(I)'2MX<sub>4</sub> or A(II)'MX<sub>4</sub> structures (n=1), respectively (Figs. 4b and 4c). Common examples of monovalent A(I)'1+ are butylammonium (C<sub>4</sub>H<sub>9</sub>NH<sub>3</sub><sup>1+</sup> or BA<sup>1+</sup>) or phenethylammonium (C<sub>6</sub>H<sub>5</sub>(CH<sub>2</sub>)<sub>2</sub>NH<sub>3</sub><sup>1+</sup> or PEA $^{1+}$ ), and divalent A(II) $^{\prime 2+}$  are 3-(aminomethyl)piperidinium (3AMP $^{2+}$ ) or 4-(aminomethyl)piperidinium  $(4AMP^{2+})$ .[32, 35]  $M^{2+}$  is  $Pb^{2+}$ ,  $Sn^{2+}$ ,  $Ge^{2+}$ ,  $Cu^{2+}$ ,  $Cd^{2+}$ , etc. or combinations of monovalent (Ag $^{1+}$ ) and trivalent (Bi $^{3+}$ , Sb $^{3+}$ ) cations. In the A(I) $^\prime{}_2MX_4$  structure the octahedra layers are staggered, with a van der Waals gap, whereas in the A(II)'MX4 structure the octahedra are aligned, and are bonded directly. [32, 35] By introducing additional small A<sup>1+</sup> cations, more than one octahedra layer can be introduced to result in fractional increase in dimensionality (n=2, 3...). A(I)'2AM2X7 and A(I)'2A2M3X10 are examples of n=2 and n=3, respectively, so-called Ruddlesden-Popper (R-P) phases with van der Waals gaps (Fig. 4b), and a general formula A(I)'<sub>2</sub>A<sub>(n-1)</sub>M<sub>n</sub>X<sub>(3n+1)</sub>. [32, 35] Similarly, examples of Dion-Jacobson (D-J) without the van der Waals gaps are A(II)'AM<sub>2</sub>X<sub>7</sub> and A(II)'A<sub>2</sub>M<sub>3</sub>X<sub>10</sub> for n=2 and n=3, respectively (Fig. 4c), and a general formula  $A(II)'A_{(n-1)}M_nX_{(3n+1)}$ . There is a third variation of LD structure unique to MHPs: alternating cation in interlayer space (ACI) with a general formula  $A(I)'A_nM_nX_{(3n+1)}$ .[35]

### Synthesis and processing of MHP thin films

Enormous amount of research has gone into developing approaches and methods for depositing high quality MHP thin films, which has been key to the success of PSCs. Majority of the processing has been solution based, where the basic approach begins with obtaining a precursor, which is a clear liquid solution of the desired MHP ingredients in a solvent or a combination of solvents, together with certain additives. The solution-processing is broadly divided into so-called 'one-step' and 'two-step' approaches. In 'one-step' approach the solution is deposited as a thin film on the substrate typically using spin-coating. The liquid film is crystallized *via* supersaturation into either the MHP phase or a solid adduct; supersaturation is achieved by heating, anti-solvent treatment, gas-blowing, *etc.* Post-heat-treatment at a moderate temperature

(100-150 °C) is necessary to complete the crystallization process in already crystallized MHP thin films and solid adduct films, or to crystallize the liquid film itself. The 'two-step' approach entails sequential deposition of two precursors and their interdiffusion and reaction. The overall goal of solution-processing is to attain high-crystallinity, phase-pure MHP thin films with the desired composition, morphology, microstructure, and thickness. There are several variations of this basic solution-processing approach, and are reviewed comprehensively by Dunlop-Shohl, *et al.*<sup>[33]</sup> Vapor-based approaches are also used for the deposition of MHP thin films, where the 'one-step' method entails single-source or dual-source evaporation, and the 'two-step' method entails sequential vapor deposition. Vapor-based approaches offer certain advantages over solution-processing approaches such as better control over thin-film morphology and composition. [33, 36]

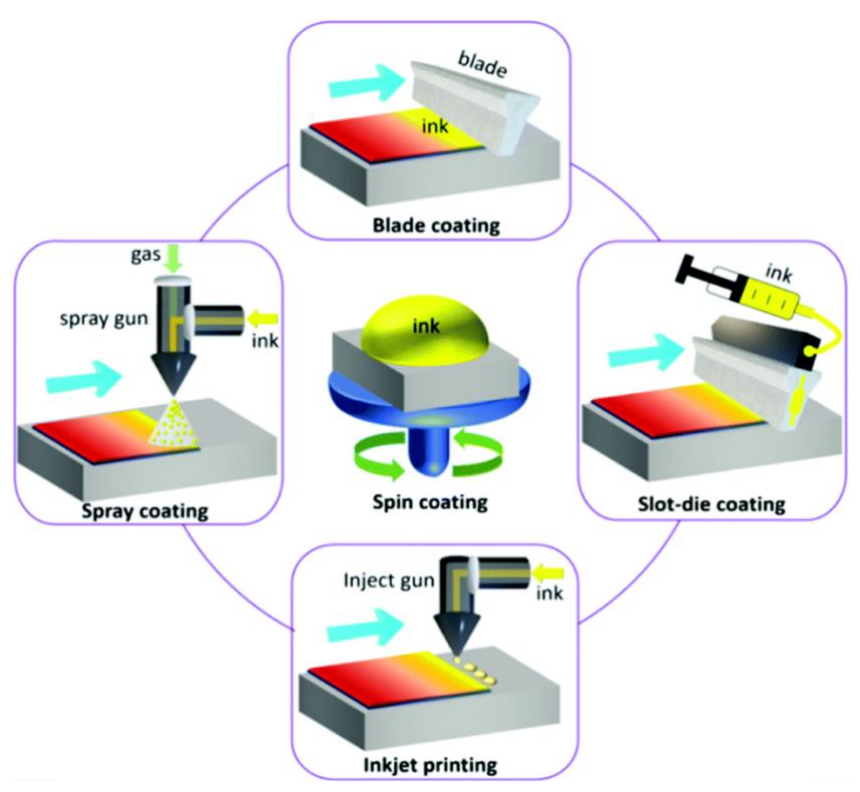


**Figure 5**. Schematic illustration of various scalable solution-processing methods, together with spin-coating, for the deposition of MHP thin films.<sup>[37]</sup> Not to scale. Reproduced with permission.

Scale-up of high-quality pinhole-free MHP thin-film processing remains a significant challenge, where the overall goal is to achieve high uniformity of the aforementioned attributes (high-crystallinity, phase-purity, composition, morphology, microstructure, thickness) over tens of cm<sup>2</sup> area for perovskite solar modules (PSMs). Here spin-coating is limited to smaller areas and it

may not be amenable to scaled-up manufacturing, and also there are concerns regarding the low material yield and the use of undesirable solvents such as dimethylformamide (DMF) and dimethylsulfoxide (DMSO). Therefore, other solution-based scalable methods that use relatively benign solvents are gaining popularity, which include (Fig. 5): (i) blade-coating, (ii) slot-die-coating, (iii) spray-coating, (iv) ink-jet printing, and (v) dip-coating, some of which may be amenable to continuous manufacturing processes such as roll-to-roll on flexible plastic substrates. [37-40] Since the processing steps typically used in spin-coated thin films, such as antisolvent treatment, extended post-heat-treatments, *etc.*, cannot be adopted here easily, other innovative approaches such as: (i) heated-substrate, [41] (ii) 'gas-knife' blowing, [42] (iii) photon-flash annealing, [43] and (iv) plasma-annealing, [44] are being pursued. Progress is also being made in vapor-based and vapor-assisted scalable processing of MHP thin films. [36, 45]

### MHP thin-film microstructures

MHP thin films in PSCs are invariably polycrystalline, and as such they have a microstructure comprising single-crystal bulk grains, and grain boundaries (GBs) where those grains are bonded together to form 2D defects of high disorder. [33, 46, 47] The microstructure in MHP thin films is the result of the nature of their synthesis using solution- and/or vapor-based methods, where single-crystal nuclei form, grow, and eventually coalesce to form a GB-network. [47] Figures 6a-g present scanning electron microscope (SEM), transmission electron microscope (TEM), highresolution TEM, and photocurrent atomic force microscope (AFM) images showing a diversity of microstructures and GBs. [48-54] Although GBs are narrow 2D 'channels' compared to the vast grain bulk and 2D grain surfaces, GBs have an outsized effects. The detrimental effects of GBs include: [47] (i) photocarriers recombination; (ii) photocarriers blocking and scattering; (iii) facile ion migration along GB 'highways'; (iv) facile ingression of moisture and oxygen; and (v) poor fracture toughness. However, GBs also offer some positive benefits such as:<sup>[47]</sup> (i) passivation of defects; (ii) functionalization; and (iii) smoother surfaces in fine-grained films. In this context, extending the famous quotation by Nobel laureate Wolfgang Pauli [55] it has been said: "God made the bulk; surfaces were invented by the devil; and grain boundaries are the creation of Dr. Jekyll and Mr. Hyde." [47] In any case, generally, it is desirable to have large average grain size (i.e. low GB-density), several times the film thickness to minimize detrimental effects of GBs. However, this presents a processing challenge due to drag on GB motion imposed by the omnipresent GB-

grooves, resulting in grain-growth stagnation. This can be overcome using innovative approaches such as phase-transformation-induced grain growth in FAPbI<sub>3</sub> [56] or MA gas-induced grain growth in MAPbI<sub>3</sub>, [50] but there are several others. In this context, there is increasing awareness regarding the detrimental effects of other 2D defects within the single-crystal bulk grains, such as stacking-faults, twin-boundaries, domain-boundaries, and polytype-boundaries. [57] Although these 2D defects are not as disordered as regular GBs, they are more numerous and can have dominating effects on MHP thin film properties.

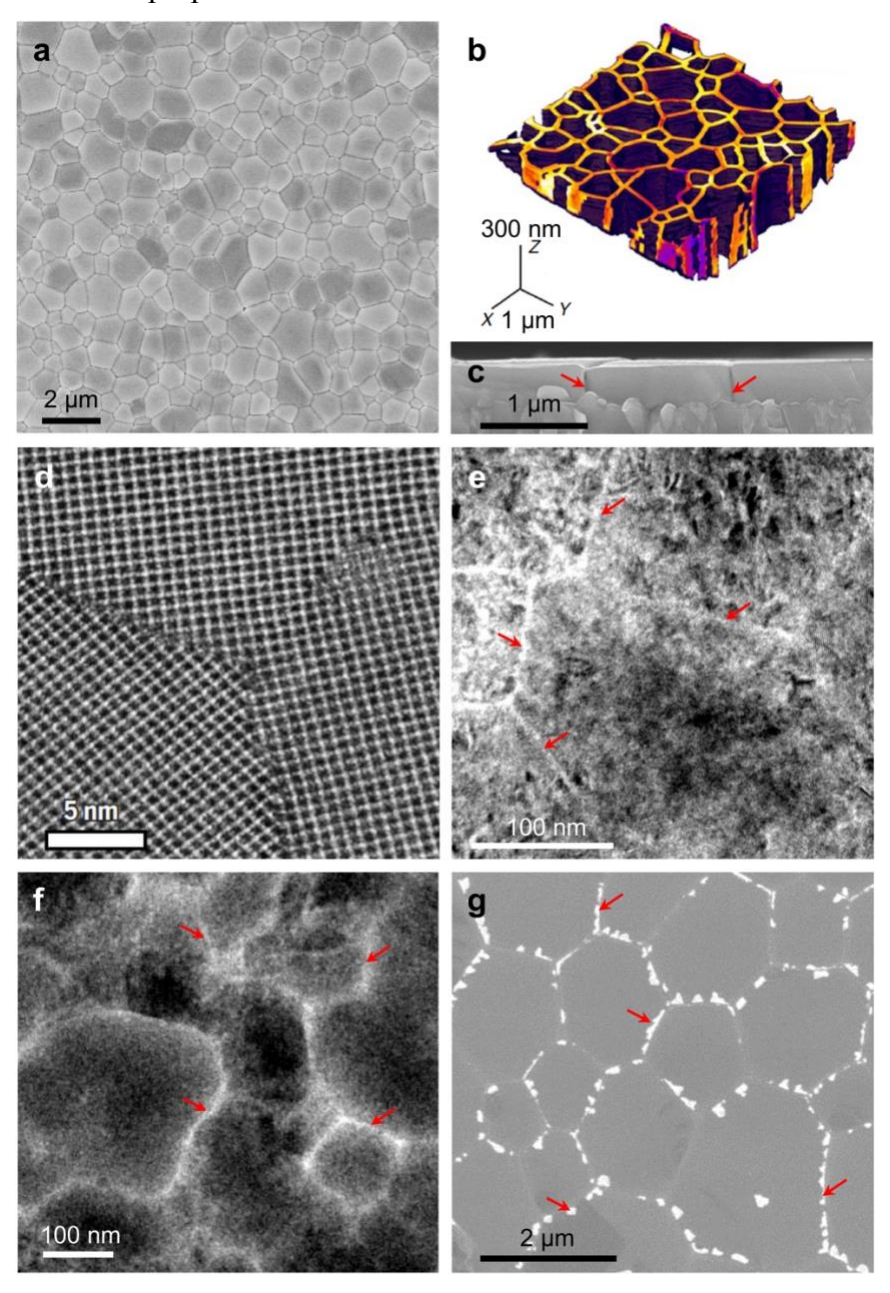


Figure 6. (a) Top-view SEM image of a MAPbI<sub>3</sub> MHP thin film with 0.9 μm average grain size.<sup>[48]</sup> (b) 3D

photocurrent AFM mapping image of a MAPbI<sub>3</sub> MHP thin film.<sup>[49]</sup> (c) Cross-sectional SEM image of a MAPbI<sub>3</sub> MHP thin film with 1.7 μm average grain size.<sup>[50]</sup> (d) High-resolution TEM image of clean GBs in a free-standing FAPbI<sub>3</sub> MHP thin film.<sup>[51]</sup> (e) TEM image of a free-standing MAPbI<sub>3</sub> MHP thin film with GBs functionalized by a tri-block copolymer.<sup>[52]</sup> (f) TEM image of a free-standing MAPbI<sub>3</sub> MHP thin film with grains encapsulated by SiO<sub>x</sub>.<sup>[53]</sup> (g) SEM image of (FAPbI<sub>3</sub>)<sub>0.7</sub>(CsSnI<sub>3</sub>)<sub>0.3</sub> MHP thin film with CaF<sub>2</sub> at GBs.<sup>[54]</sup> Red arrows indicate GBs. Reproduced with permission.

In polycrystalline MHP thin films there is evidence that favoring certain grain crystallographic orientations (texture) may be at least as important as grain size. Different facets of grains have also shown different levels of effectiveness in their PV parameters. Also, it has been shown that certain facets in MHP thin films degrade faster than others. Also, it has been shown that certain facets in make more important in LD perovskite thin films (*e.g.* R-P and D-J). The pronounced anisotropy of their crystal structures results in anisotropy of the carrier mobility, wherein transport is generally easy along the planes of corner-sharing metal halide octahedra but not across them. However, there are questions regarding the phase purity of LD MHPs (n>1); it has been shown that most films are typically unknown mixtures of 3D and LD phases.

MHP quantum dots (QDs) afford some unique optoelectronic properties, and they can also be assembled into thin films with unique microstructures for PSCs. [63, 64] Since these microstructures are assembled, rather than evolved, the QDs-stabilizing surface ligands end up forming the GBs between tightly packed single-crystal QD grains.

# **PSC** functional layers

High-performing PSCs have at least four basic functional layers, in addition to the sandwiched MHP thin film, that are deposited sequentially, *viz* (Figs. 2a-2c): (i) TCO front electrode, (ii) ETL, (iii) HTL, and (iv) rear electrode. The materials for these layers are chosen/tuned based primarily on their electronic properties *vis-à-vis* MHP to achieve energy-level offsets (band alignment) shown in Figs. 7a and 7b for *n-i-p* and *p-i-n* PSCs, respectively. Here the MHP is generally an intrinsic (*i*) semiconductor, while the ETL and HTL are *n-* and *p-*type electronand hole-selective semiconductors, respectively. Also, processing methods are a major materials-selection consideration, where sequential deposition of each high-quality layer must be compatible with not only the previous layer but also the cumulative multilayer stack.

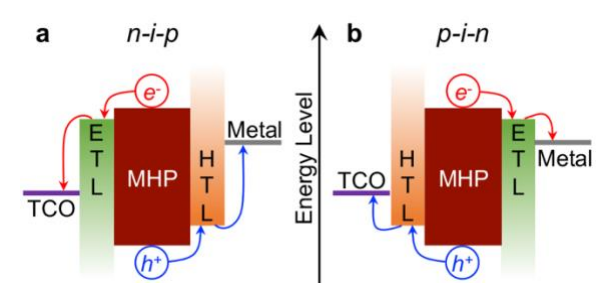


**Figure 7**. Schematic illustration of energy level diagrams in PSCs, with  $e^-$  and  $h^+$  pathways: (a) n-i-p and (b) p-i-n. Not to scale.

In both *n-i-p* and *p-i-n* PSCs, the front electrode must be transparent, and the most commonly used TCO for that purpose is indium-tin oxide (ITO) or fluorinated-tin oxide (FTO), deposited on glass or plastic substrates, where a combination of high transparency and low sheet resistance is desirable. ITO typically has lower sheet resistance, but FTO seems to be more robust chemically. The rear electrode is typically thermally-evaporated reflective thin layer, or patterned fingers, of a noble metal: Au or Ag. Due to concerns regarding the high cost of noble metals and their diffusion into other PSC layers, other metals such as Cu and Al are being considered. Carbon electrodes (carbon black, graphite, graphene, nanotubes) are also gaining popularity due to their low cost, tunability, and protection against moisture. The rear electrode needs to be transparent or semitransparent for bifacial PSCs which collect ground albedo from the rear to boost their PCEs, and also for 'top' PSCs (Fig. 2d) in four-terminal tandem PVs. Here the rear electrode is a TCO (*e.g.* indium-zinc oxide (IZO) or aluminum-zinc oxide (AZO)) which is typically deposited using sputtering without damaging the underlying layers. Networks (mats) of metal nanowires (*e.g.* Au, Ag, Cu, Ni) have also been investigated as semitransparent rear electrodes. [65]

In *n-i-p* PSCs, the ETL on TCO-coated substrate is compact and with high optical transparency. The vast majority of studies use inorganics such as TiO<sub>2</sub> or SnO<sub>2</sub>, although other oxides such as ZnO, Nb<sub>2</sub>O<sub>3</sub>, WO<sub>x</sub>, CeO<sub>x</sub>, ZnSnO<sub>4</sub>, BaSnO<sub>3</sub>, *etc*. have also been investigated.<sup>[66]</sup> TiO<sub>2</sub>-based ETLs have good band alignment with respect to MHPs, but they suffer from relatively lower *n*-type conductivities. Also, TiO<sub>2</sub> can serve as a UV-photocatalyst, which can promote the degradation of the MHP thin film in contact with the ETL. In this context, SnO<sub>2</sub> is gaining popularity because of its lower photocatalytic activity, higher *n*-type conductivity, and better band alignment with mixed MHPs.<sup>[67, 68]</sup> Also, high-quality SnO<sub>2</sub> ETLs can be deposited using low-temperature (<180 °C) processes, which is helping break new ground in the area of high-PCE

flexible PSCs on plastic substrates.<sup>[67]</sup> In *n-i-p* PSCs, the HTL is typically an organic which can be deposited on the MHP thin film without damaging it in anyway. The most popular organic HTL is the small-molecule spiro-OMeTAD (2,2',7,7'-tetraki{N,N-di(4-methoxyphenyl)amino}-9,9'-spirobifluorene), which needs to be doped with a Li salt such as bis(trifluoromethane)sulfonimide (LiTFSI).<sup>[69]</sup> The excellent *p*-type conductivity of doped spiro-OMeTAD affords thinner HTL, but the high cost and the migration of the highly mobile Li dopant to the other layers are important concerns. Numerous other small-molecule HTLs have also been investigated. Polymer HTLs are also commonly used, with the most widely studied ones being (doped or undoped):<sup>[69]</sup> poly{bis(4-phenyl)(2,4,6-trimethyl-phenyl)amine} (PTAA), poly(4-butylphenyl-diphenyl-amine) (PolyTPD), and poly{3-hexylthiophene-2,5-diyl} (P3HT). Once again, numerous other polymer HTLs have been investigated. Inorganic HTLs that can be deposited without damaging the MHP thin film include CuI, Cu<sub>2</sub>O, CuPc, CuSCN, MnS, *etc*.

In p-i-n PSCs, the most common organic HTLs deposited on TCO-coated substrates include poly(3,4-ethylenedioxythiophene) polystyrene sulfonate (PEDOT:PSS), PTAA, and P3HT. The most common inorganic HTLs are Ni-based and Cu-based oxides, which typically need higher temperatures for deposition. Some of these HTLs absorb strongly in the blue region of the solar spectrum, which can be alleviated by using molecular layers as HTLs. In this context, carbozole-based self-assembled monolayers (SAMs) have been shown to be highly effective HTLs, which include {2-(9H-carbazol-9-yl)ethyl}phosphonic acid (2PACz) and {2-(3,6dimethoxy-9H-carbazol-9-yl)ethyl} phosphonic acid (MeO-2PACz),<sup>[70]</sup> but there are several others. Organic ETLs are preferred in *p-i-n* PSCs because they can be deposited on the MHP thin film using gentle processing conditions. Also, organic ETLs are more tunable, and they passivate the MHP thin film surface very effectively. The most commonly used ETLs are fullerene-based (e.g. C<sub>60</sub> or {6,6}-phenyl-C<sub>61</sub>-butyric acid methyl ester or PC<sub>61</sub>BM) and they are generally deposited by thermally-evaporation.<sup>[19]</sup> A very thin buffer layer is typically needed between PC<sub>61</sub>BM and the rear electrode to block holes and reduce photocarrier recombination at that interface; buffer-layer materials include bathocuproine (BCP), Ti(Nb)Ox, SnOx, and LiF.[71] Inorganic ETLs (e.g. TiO2, SnO2, ZnO, etc.) are also used, typically in conjunction with organic ETLs as multilayers or hybrids.<sup>[71]</sup>

# **Interfacial engineering in PSCs**

Nobel laureate Herbert Kroemer famously said "the interface is the device" [72] — this certainly rings true of PSCs. There is a minimum of four interfaces in a typical PSC (Fig. 2): (i) front TCO electrode / ETL or HTL; (ii) ETL or HTL / MHP; (iii) MHP / HTL or ETL; and (iv) HTL or ETL/rear electrode. There are additional interfaces in more complex devices such as two-terminal tandem PVs, although interfaces (ii) and (iii) above are the most studied. This has presented, and continues to present, vast opportunities for interfacial engineering to attain the desired performance in PSCs.[73-75] Generally, the main purposes of interfacial engineering are to:[74,75] (i) modulate band alignment between adjacent layers; (ii) passivate interfacial defects and reduce dissipative recombination; (iii) achieve efficient and balanced photocarriers extraction to reduce hysteresis; (iv) improve the quality of the subsequently deposited layer; (v) prevent adverse chemical reactions between layers; (vi) provide protection against environmental degradation; and (vii) improve mechanical adhesion. The importance of the latter has only recently been recognized from a mechanical reliability and durability standpoint.[76-83]

Interfacial engineering entails many materials and approaches, and they are specific to the interface in question. Typically, the following materials, or their combinations, are incorporated at interfaces (also referred to as buffer layers):<sup>[74, 75]</sup> (i) small organic molecules, including fullerene derivatives and salts; (ii) polymers; (iii) inorganic molecules and salts; (iv) inorganic layers; (v) QDs; (vi) 2D materials; (vii) LD MHPs; and (viii) SAMs. The incorporation of the latter is gaining popularity because SAMs are perhaps the most versatile and tailorable, and they can be used to accomplish multiple afore-stated purposes simultaneously.<sup>[75, 80, 84, 85]</sup> Also, SAMs are amenable to room-temperature scalable processing. In the case of two-terminal tandem PVs (Fig. 2e), an interconnection layer is introduced at the interface between the two solar cells, which is typically made of a very thin TCO (*e.g.* ITO, IZO) or metal/ETL bilayer (*e.g.* Au/SnO<sub>2</sub>).<sup>[22]</sup> Once again, like in the case of functional-layers deposition in PSCs, compatibility of sequential interfacial-layers deposition processes is also a major consideration.

# **PSC** performance

As seen in Fig. 1, there has been an impressive rise in the PCE of PSCs, but there are a few PV performance features that are unique to PSCs, and are as follows. First, PSCs show hysteretic *J-V* response in reverse and forward scan (and also scan rate), some more than others. For example,

Fig. 8a presents current density (J) - voltage (V) plots for a state-of-the-art PSC showing negligible hysteresis, with the highest PCE of 26.08% in reverse scan and 25.70% in forward scan. [86] Figure 8b shows an example of an early PSC with more pronounced hysteresis, where the reverse- and forward-scan PCEs are 15.5% and 10.2%, respectively. [87] This raises concerns regarding appropriate protocol for measuring and reporting PCEs, which are partly addressed by reporting stabilized J and PCE ( $\eta$ ) at maximum-power-point bias (Fig. 8b inset). [87] Several reasons for this type of behavior have been offered in the literature: [88] slow transient capacitive current; dynamic trapping and de-trapping processes of charge carriers; and band bending due to ion migration or ferroelectric polarization. Achieving balanced extraction of electrons and holes via interfacial engineering generally results in little to no hysteresis. [88]

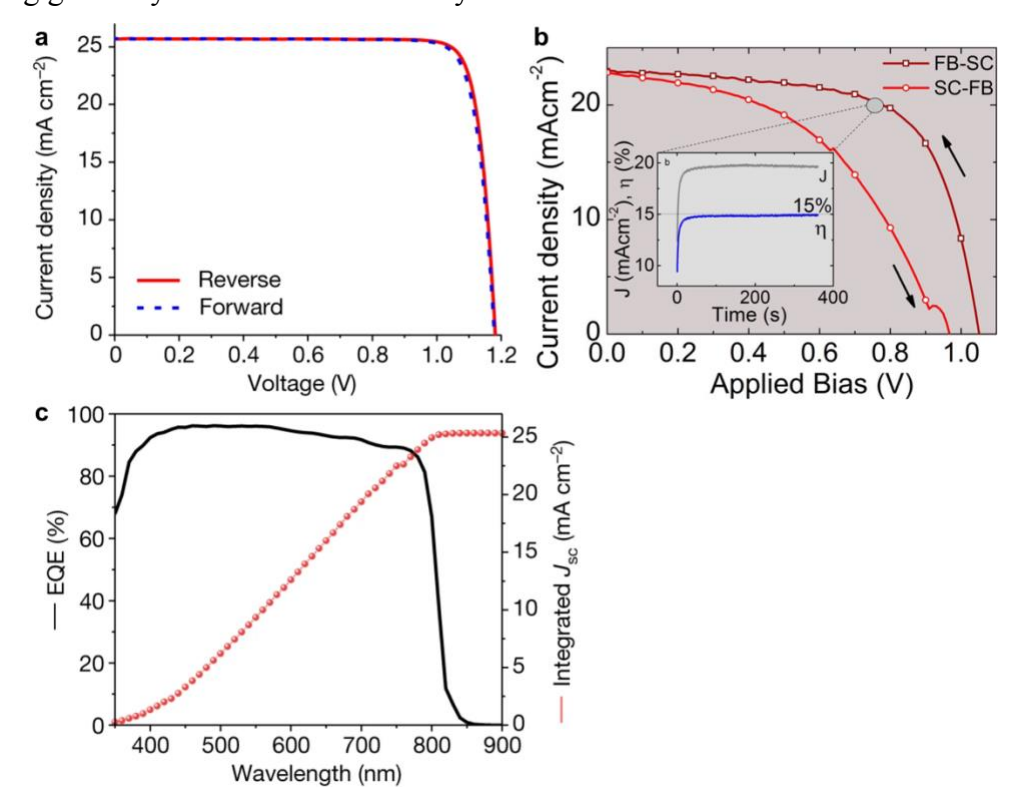


**Figure 8.** (a) J-V responses of a PSC in forward and reverse scans. [86] (b) J-V responses of a PSC in forward and reverse scans. Inset: stabilized J and PCE ( $\eta$ ) output. [87] (c) EQE and integrated-J<sub>SC</sub> spectra of the PSC in (a). [86] Reproduced with permission.

Second, the external quantum efficiency (EQE) spectrum in Fig. 8c for the PSC in Fig. 8a shows very high EQE, with maximum value reaching ~97%. This unusual behavior has been subject of several investigations, and it is generally accepted that the high refractive index of MHP

thin film is responsible for more efficient transmission of light into it.<sup>[89]</sup>

Third, PSC with current certified record PCE of 26.0% in Fig. 1 has the following PV parameters: short-circuit current density ( $J_{SC}$ ) 26.00 mA.cm<sup>-2</sup>, open-circuit voltage ( $V_{OC}$ ) 1.19 V, and fill factor (FF) 0.84. By comparison, the heterojunction (HJT) silicon solar cell with current certified record PCE of 26.81% (LONGi) in Fig. 1 has  $J_{SC}$  41.45 mA.cm<sup>-2</sup>,  $V_{OC}$  0.7514 V, and FF 0.8607. The  $V_{OC}$  of PSCs is extraordinarily high, and it is, in fact, the highest among all current certified-record single-junction solar cells technologies in Fig. 1. Figures 9a and 9b show PCE and  $V_{OC}$  of various solar cell technologies, including PSCs with different bandgap ( $E_g$ ) MHPs, as a function of  $E_g$ . Note that high-PCE PSCs have  $V_{OC}$  very close to the theoretical limit. [90]

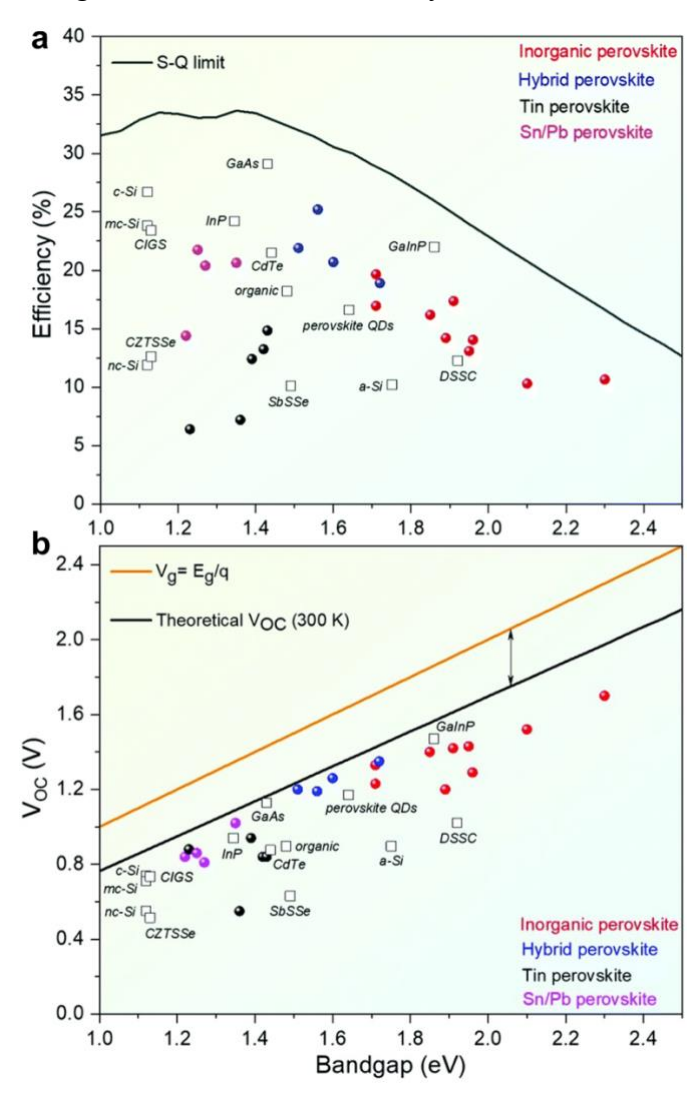


**Figure 9.** Plots for PSCs using various MHPs, and other types of solar cells: (a) PCE vs.  $E_g$  and (b)  $V_{OC}$  vs.  $E_g$ . The S-Q limit curve is indicated in (a), and theoretical  $V_{OC}$  and  $E_g/q$  lines are indicated in (b). [90] Reproduced with permission.

Fourth, the PCEs of single-junction PSCs in Fig. 1 and Fig. 8a are for very small areas, typically <0.1 cm². For example, PSC with current certified record PCE of 26.0% (ISCAS) in Fig. 1 has a 0.0746 cm² area, whereas the single-crystal and HJT silicon solar cells with current certified record PCEs of 26.1% (ISFH) and 26.81% (LONGi), respectively, in Fig. 1 have 3.9857 cm² and 274.4 cm² areas. [6] In this context, the "Solar Cell Efficiency Tables" complied by Green, *et al.* [91] over the past 30 years list the latest certified records for solar cells with at least 1 cm² area. In which case, for PSC with 1.062 cm² area the current certified record PCE reduces to 23.7% (USTHefei). [91] The tandem PV with current certified record 33.7% PCE (KAUST) in Fig. 1 has 1.0035 cm² area. [6] This highlights the upscaling challenges PSCs face, and are discussed later in this paper in the context of PSMs.

# **PSC** stability

Poor operational stability of PSCs has been an overriding concern over the past few years, and tremendous amount of effort is being put into addressing this issue.<sup>[4, 92, 93]</sup> The factors determining the stability of PSCs during their operation include the following, but are not limited to: (i) structural stability of the MHP and defects; (ii) intrinsic stability of the functional layers; (iii) interlayer interactions and unintended reactions; (iv) coupled phenomena with external stimuli: environment (H<sub>2</sub>O, O<sub>2</sub>), heat, light, and electric field; and (v) mechanical-stresses and properties evolution. The latter is the least studied, and it is discussed in a separate section in this paper in the context of mechanical reliability.

The low formation energies of MHPs which make them amenable to near-room-temperature processing also make them less stable. [33] Some of the MHP compositions have barely negative enthalpies, while some others are above zero. [94] Thus, MHPs are always at the cusp of instability, and are barely stabilized by effects such as configurational entropy and kinetic trapping. As mentioned earlier, the AMX3 perovskite structural stability is empirically determined by the Goldschmidt-tolerance (0.8<t<1) and octahedral (0.4< $\mu$ <0.9) factors criteria. Therefore, one approach that has been remarkably successful is alloying at all three sub-lattice sites (A, M, X) to bring the two 'effective' factors well within their respective ranges. [95, 96] However, it should be borne in mind that the Goldschmidt-tolerance and octahedral factors criteria are empirical, and they are not uniformly applicable in the case of MHPs. [34, 97] Other approaches used to stabilize the

MHP structure include the elimination of organic A<sup>1+</sup> cation and the use of additives (*e.g.* chloride, fluoride, formate, fluoroborate).<sup>[4]</sup> GBs and surfaces of MHPs, with their high defect densities, are particularly susceptible to destabilization, which is typically mitigated through GB-passivation and the use of interfacial layers discussed earlier. Among ETL, HTL, and electrode layers, inorganic ones are generally quite stable intrinsically, whereas some organic layers may suffer premature destabilization. However, interlayer interactions, and coupling with multiple external stimuli, are factors that can dominate PSCs stability, and are highlighted next.

At the center of these effects is the facile ion-migration in MHPs at room temperature. [98] Thermally-activated, defect-mediated ion-migration (self-diffusion, foreign-species diffusion) in MHP is driven by concentration gradient, electric field, and/or strain field. The weak bonding (i.e. low formation energies) in MHPs, which offers low resistance to diffusion, together with the abundance of point defects makes ion-migration in MHPs facile (i.e. low activation energies). MHP decomposition products (i.e. A<sup>1+</sup>, M<sup>2+</sup>, X<sup>1-</sup>) can diffuse relatively easily through the lattice, mediated by defects such as vacancies  $(V_X^{\bullet}, V_{A'}, V_{M''})$  and interstitials  $(X_i', A_i^{\bullet}, M_i^{\bullet \bullet})$ , and into adjacent layers and/or escape the system, resulting in the permanent degradation of the MHP thin film. Ion-migration along GBs can be significantly faster; however, effective mass flux is limited by the relatively small areal cross-section of GBs compared to that of the bulk lattice. Similarly, ionic-reaction products due to interaction with the adjacent layers and/or reaction with environmental species (e.g. H<sub>2</sub>O, O<sub>2</sub>) can also escape the system. Here, GBs prove to be more potent as they allow easy ingress of the environmental species, and typically the degradation is initiated at GBs. [57, 99] Applied and/or built-in electric field, which is ubiquitous in a solar cell, add to the concentration-gradient driving force, and strain fields have a similar effect. Light, which is also ubiquitous in a solar cell, appears to have multiple undesirable effects on ion-migration. [4] First, it 'softens' the MHP lattice, thereby making ion-migration relatively easier. Second, photocarriers can screen columbic attraction between ions, which can promote ion-migration. Third, photocarriers alter the electric field and influence ion-migration. Fourth, photocarriers can oxidize or reduce the diffusing ionic species. One of the most-well-known light-effects on ionmigration is the separation of halide phases in high-bandgap mixed-halide MHP thin films that are so important for tandem PV application.<sup>[100, 101]</sup> Finally, any polymer layers within the PSCs are likely to degrade over time from to the UV component of the solar spectrum.

Given the critical importance, there has been intense effort worldwide to mitigate

degradation of PSCs during operation and improve their operational stability. But the community needed to build a consensus around how best to assess and report PSC operational stability. This is because there are many peculiarities in the stability behavior of PSCs, and established protocols and standards for commercial PV panels cannot be applied to PSCs directly. For example, PSCs tested under continuous illumination under maximum-power-point tracking (MPPT) conditions (lower voltage) degrade less rapidly (Fig. 10a) than PSCs biased under high voltage (Fig. 10c), but they degrade more rapidly compared to intermittent J-V testing (Fig. 10a). [102-104] PSCs also show initial PCE 'burn-in' or non-monotonic PCE degradation over time, which creates issues regarding how to define the initial PCE and estimate T<sub>80</sub>, a useful operational-stability metric: duration (time) until retention of 80% of the initial PCE. There are also questions around continuous-illumination testing or cyclic testing (to simulate day and night cycles). For example, PSC partially recover their PCE in the dark (Fig. 10b). [104, 105] (Such 'healing' has other important implications, including unique suitability of PSCs for outer-space applications. [106, 107]) To that end, a Consensus Statement based on International Summit on Organic Photovoltaic Stability (ISOS) protocols was published in 2020,[104] and it is being adapted to some extent by the community worldwide. For example, Figs. 10d and 10e illustrate schematically protocols for estimating T<sub>80</sub>, and also T<sub>880</sub> (duration until retention of 80% of a certain PCE). [104] Figure 10f shows examples of operational-stability data for epoxy-encapsulated PSCs, tested using the ISOS-L1 protocol. [108] Still, testing protocols and reporting in current literature papers vary across labs, and meaningful comparisons of results is not always straightforward.

The efforts to improve PSC operational stability encompass a myriad combinations of various approaches. [4, 77, 98] The main approaches include, but are not limited to the following. (i) Engineer MHP compositions to stabilize MHPs, and use of dopants and additives to reduce defect concentration. The latter also helps slow down ion-migration. (ii) Passivate MHP surfaces and interfaces using various passivating molecules and treatments. (iii) Use more stable functional layers, which include polymers and inorganics. (iv) Incorporate thin buffer layers between the different layers to reduce interlayer reactions. These films, which comprise inorganics, polymers, 2D materials, LD MHPs, *etc.*, also help protect the layers against ingression of environmental species. (v) Grow grains in MHP thin films, and functionalize GBs, to slow down ion-migration and protect GBs. (vi) Use multi-layer internal and external encapsulation for effective sealing of the PSC from the environment with minimum damage to the PSC during encapsulation. (vii)

Reduce residual stresses in the MHP thin film and increase adhesion toughness of the interfaces.

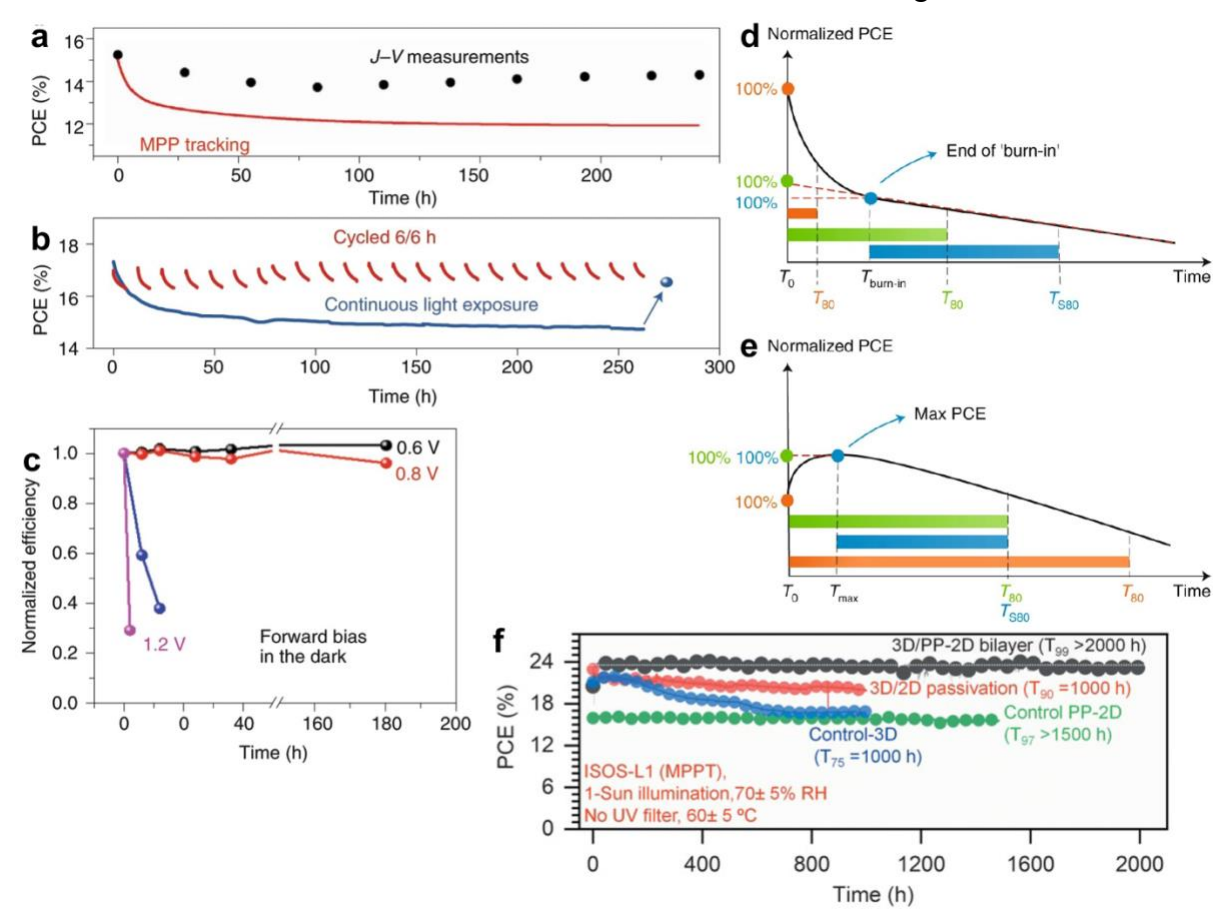


**Figure 10.** (a) PCE extracted from continuous MPP tracking (red curve) versus periodic *J-V* forward scans.<sup>[102]</sup> (b) PCE evolution of PSCs exposed to continuous (blue curve) or cycled (6/6 h, red curves).<sup>[105]</sup> (c) Normalized PCE changes of PSCs exposed to different forward bias in the dark.<sup>[103]</sup> (d)-(e) Common practices in the T<sub>80</sub> and T<sub>880</sub> estimations.<sup>[104]</sup> The black curves show schematically how PCE evolves with ageing time in the case of 'burn-in' effect (d) and in the case of nonmonotonic PCE (e). (f) Operational-stability data for various epoxy-encapsulated PSCs tested using the ISOS-L1 protocol.<sup>[108]</sup> Reproduced with permission.

### Perovskite solar modules (PSMs)

The PCE of single PSC decreases with increasing area because of the increasing series resistance and decreasing shunt resistance. Therefore, it is preferrable to have multiple PSCs connected together, which constitutes a perovskite solar module (PSM). The optimum number of PSCs for a given PSM area is determined by a tradeoff between the above resistance advantage and 'dead area' losses. Great progress is being made in developing PSMs, [38, 109, 110] and the current

certified record PCEs stand at 22.4% (EPFLSion/NCEUP) for 26.02-cm<sup>2</sup> area, [91] 20.6% (KIER/EPFL) for 64-cm<sup>2</sup> area.<sup>[111]</sup> and 17.9% (Panasonic) for 802-cm<sup>2</sup> area.<sup>[112]</sup> Regarding commercial-sized MHP/Si tandem PSMs, the current certified record PCE stands at 26.8% (OxfordPV) for 274.22-cm<sup>2</sup> area.<sup>[91]</sup> Figure 11a is a schematic illustration of a monolithicinterconnected PSM, where the individual PSCs are electrically isolated by successive precise scribing and scalable deposition of the layers using methods described earlier (Fig. 5). [109] (Figure 11a shows a *n-i-p* PSM, but *p-i-n* PSM architecture is very similar with the ETL and HTL swapped.) The P1 scribe in the TCO is typically made using mechanical means, whereas the P2 and P3 scribes are made using lasers. The scribing process can damage the materials in its vicinity in the so-called 'heat-affected zone,' and the newly exposed MHP vertical surfaces are susceptible to degradation, both of which adversely affect the stability of PSMs. An alternate gridinterconnected PSM architecture, reminiscent of Si solar cells, precludes the scribing process altogether and it is illustrated schematically in Fig. 11b. Here periodically placed network of 'finger' electrodes and bus bars collect the charge efficiently, however, this PSM architecture doesn't seem to be as popular. But then again, the PSM development is still in very early stages, and it is not clear which PSM architecture will eventually make it to market.

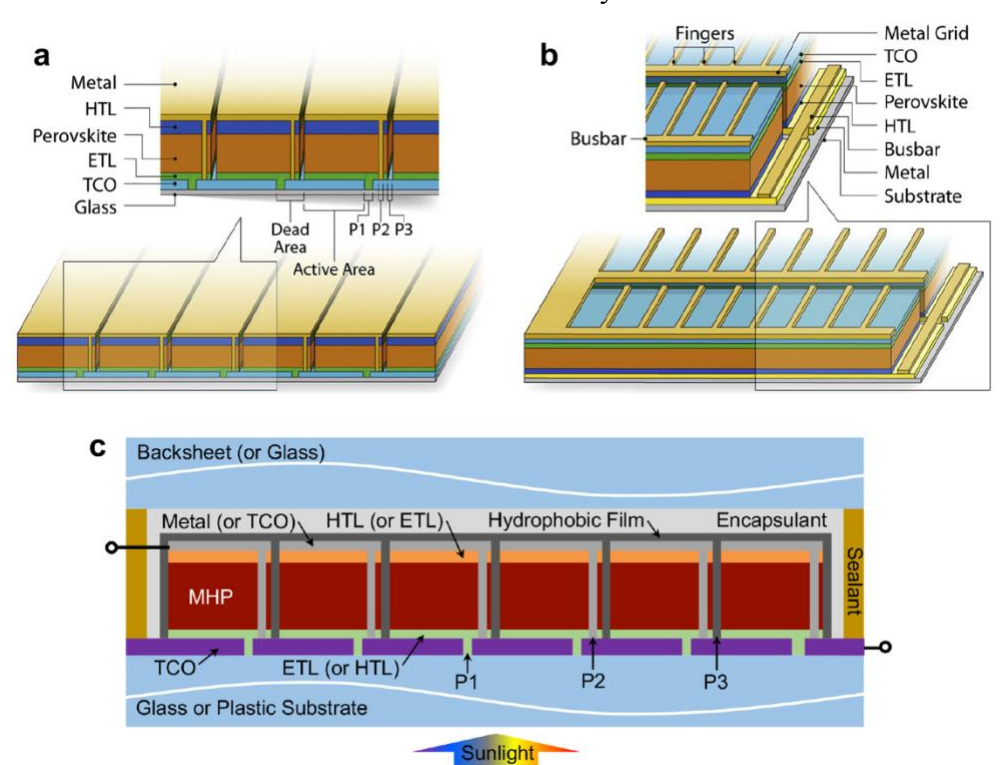


Figure 11. Schematic illustrations of n-i-p PSMs: (a) monolithic-interconnected and (b) grid-

interconnected.<sup>[109]</sup> Reproduced with permission. (c) Schematic illustration of encapsulated monolithic-interconnected PSM. No to scale.

Proper encapsulation of PSMs is essential for hermetically sealing from the environment, containing any volatile species within, and dissipating heat away from the active part. Several approaches are being investigated, but its development is also still in very early stages. Figure 11c shows a fully-encapsulated PSM schematically, but there are many other encapsulation schemes. The initial step is to deposit a hydrophobic material film around the entire PSM. The film materials include polymethylmethacrylate (PMMA), polydimethylsiloxane (PDMS), thermosetting polyurethane (PU), atomic layer deposited (ALD) Al<sub>2</sub>O<sub>3</sub>, *etc.*<sup>[113]</sup> This step addresses, to some extent, the issue related to exposure of MHP due to scribing. The PSM is then encapsulated using UV-cured epoxy or hot-lamination using ethylene vinyl acetate (EVA), Surlyn<sup>TM</sup>, polyimide (Kapton tape), polyisobutylene (PIB), or PU.<sup>[113]</sup> Additional edge sealant may be used, comprising PIB or UV-curable epoxy mixed with a desiccant such as silica or zeolite.<sup>[114]</sup> Possible damage to the PSM during the encapsulation processes and/or development of additional residual stresses post encapsulation are major concerns that need to be addressed.

# Lead toxicity

The best performing MHP-based PVs so far all contain Pb because of its unique position in the periodic table, and the electronic band structure it creates when bonded to halogen in the perovskite structure. [24] This is primarily responsible for the superior optical and defect-tolerance properties in Pb-based MHPs. [24] However, Pb is a known toxin to humans, [115] and its use in electronic devices is government regulated, although PVs are exempt in most countries and regions for the time being. [116] The main concern is the leaching of Pb out of a MHP-based solar panel into the environment. Utility-scale solar farms can be better controlled professionally to mitigate any potential danger from leached Pb; *e.g.* installation of ground-protection membranes and restricted access. According to a study, the amount of Pb added to the soil due to a broken MHP-based solar panel is expected to be extremely small over the natural abundance of Pb in the soil. [117] However, in the case of PSMs in rooftop solar panels and consumer applications the situation cannot be controlled easily. Also, the latter applications (*e.g.* backpacks, tents, portable power source, drones, *etc.*) will use lightweight flexible PSMs that are in the hands of the general public. Here the amount

of total Pb relative to the panel weight, and the amount of leached Pb are important. These estimates for PSCs on rigid (glass) and flexible (PET) substrates are presented in Figs. 12a and 12b on the basis of relative total-Pb weight and leached-Pb weight, respectively. While the European Union (EU) Restriction of Hazardous Substances (RoHS) uses the former criterion for its directive, the United States (US) Resource Conservation and Recovery Act (RCRA) uses the latter. Once again, while these do not apply to PVs for now, that could change in the future.

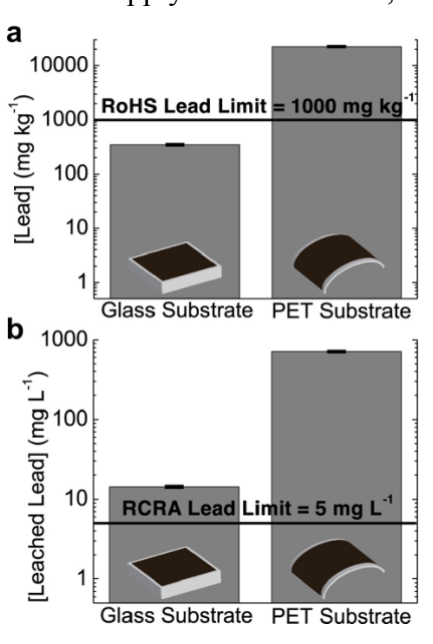


**Figure 12.** Concentration by weight of 1 inch<sup>2</sup> MHP thin films on glass and PET substrates: (a) normalized total-Pb and (b) leached-Pb.<sup>[116]</sup> The EU RoHS and US RCRA maximum limits are indicated. Reproduced with permission.

Tremendous amount of effort has gone into reducing the amount of Pb<sup>2+</sup> by alloying, or replacing Pb<sup>2+</sup> altogether in MHP-based PVs *e.g.* by Sn<sup>2+</sup> and/or Ge<sup>2+</sup>; a combination of Ag<sup>1+</sup>/Bi<sup>3+</sup> or Ag<sup>1+</sup>/Sb<sup>3+</sup>; Ti<sup>4+</sup>, *etc*.<sup>[118-122]</sup> But there are questions about the toxicity of the Pb alternatives such as Sn.<sup>[115]</sup> In any case, none of the Pb-free MHP-based PVs so far match the PCE and stability of Pb-containing ones. Perhaps the best way to get around the Pb issue is to immobilize the Pb using *in situ* approaches, such as grain encapsulation, chemical complexation, and structural integration, together with *ex situ* approaches such as adsorption and sequestration of leaked Pb within the device.<sup>[122]</sup> This should be coupled with responsible recycling and safe-disposal protocols.<sup>[121, 122]</sup> However, the issue of Pb in lightweight flexible PSMs for consumer applications still remains.

### Mechanical behavior and reliability

While great progress is being made in enhancing PCE, stability, and scalability of PSMs, any new PV technology needs to be mechanically reliable before making it to market successfully. [76, 77, 79-83] This is particularly critical in the case of PSMs because MHPs have a poor combination of basic mechanical properties, owing primarily to the weak bonding (*i.e.* low formation energies). This is compounded by the fact that PSMs are subject to significant mechanical stresses that drive failure. [77, 78, 83, 123, 124] Furthermore, there can be coupled effects on the mechanical reliability due to the ubiquitous presence of other stimuli during the operation of perovskite PVs, such as environment, light, and electric-field. [83] Despite the critical importance of mechanical reliability, this area is the least developed. [83] In this context, direct correlation between operational stability and mechanical reliability of interfaces in PSCs was demonstrated recently; [80, 82] Fig. 13a shows significant enhancement in the operational stability of PSCs, from ~700 h to ~4,000 h T80, by toughening the ETL/MHP interface using SAMs. [80] Figure 13b shows an example of flexible PSCs with extended cyclic life, from *n*70 to *n*88 for 10,000 bending cycles, when both the ETL/MHP and HTL/MHP interfaces are reinforced by SAMs and LD MHP, respectively. [82]

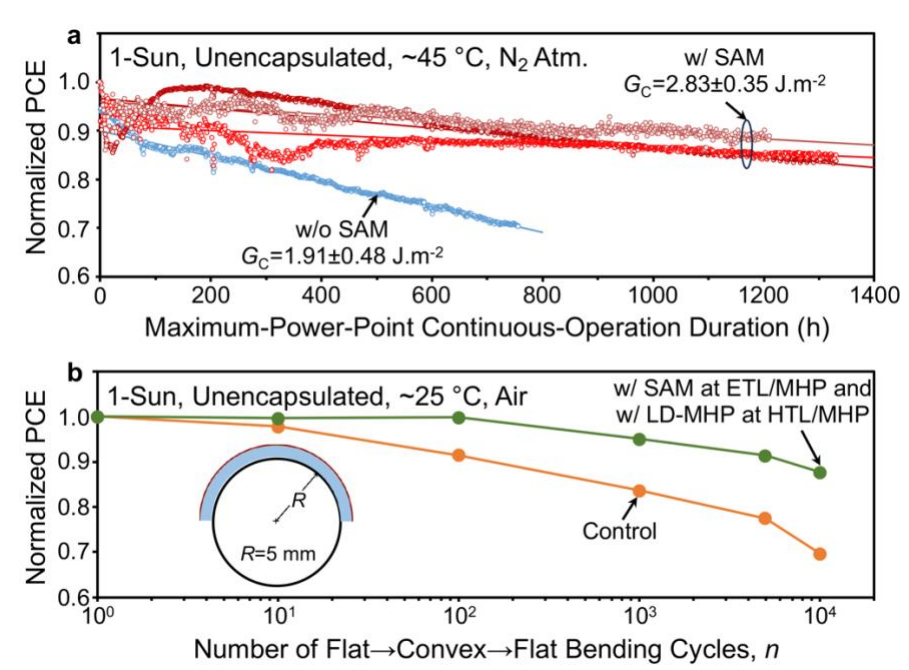


**Figure 13**. (a) Operational-stability data for PSCs without SAM and three PSCs with SAM. The lines are linear fits to the data after initial burn-in and nonmonotonic behavior.  $G_C$  is toughness of the ETL/MHP interface measured using the double-cantilever beam (DCB) method. [80] (b) Cyclic-bending performance of

flexible PSCs without interfacial reinforcements (control), and with both ETL/MHP and HTL/MHP interfaces reinforced by SAMs and LD MHP, respectively; inset: schematic illustration of the bending test (not to scale). [82] Reproduced with permission.

Figures 14a and 14b map the basic mechanical properties of MAPbI<sub>3</sub> and MAPbBr<sub>3</sub> measured reliably on high-quality single crystals: [83, 125] (i) Young's modulus (E): resistance to elastic deformation; (ii) hardness (H): resistance to plastic (localized) deformation; and (iii) fracture toughness ( $K_{IC}$ ) or toughness ( $G_C$ ): resistance to crack propagation. Note how they lie in the 'white space' in relation to general classes of materials. The single-crystal values are expected to be upper bounds, and those for MHP polycrystalline thin films relevant to PSCs and PSMs are expected to be lower. The time-dependent (e.g. creep) and cycle-dependent (e.g. fatigue) mechanical properties of MHPs also await detailed studies. Another critically important property is the mechanical adhesion toughness ( $G_{\mathbb{C}}$ ) of the different interfaces. While mechanical properties may be viewed as materials 'defense,' the mechanical stresses are the 'offense' that drive failure. Macroscopic, long-range mechanical stresses in the MHP thin film that drive failure ('offense') arise from two main sources.<sup>[77, 78, 83, 123, 124]</sup> First is equi-biaxial residual tensile stress in the MHP thin film due to its thermal-expansion mismatch with the relatively massive substrate. Second is externally applied stresses, which add to the residual stress, as a result of quasi-static loading (e.g. stretching, bending, twisting), cyclic loading (e.g. wind, vibrations), and/or impact loading (e.g. hail, collision). Additional sources of mechanical stress include those developed during manufacturing processes such as scribing, encapsulation, etc. Another unique aspect of MHPs is the ability of cracks to heal under moderate compressive stress or mild heat-treatment, leading to the axiom: "What is easy to 'make' (solution-processing), is easy to 'break' (fracture), but is also easy to 'fix' (crack-healing)." [126] Thus, the interplay between mechanical properties, driving stresses, and failure mechanisms which determine the mechanical reliability of MHPs, PSCs, and PSMs is complex, and there are vast challenges and opportunities in addressing these issues, as described in a recent perspective article (Fig. 15).[83]

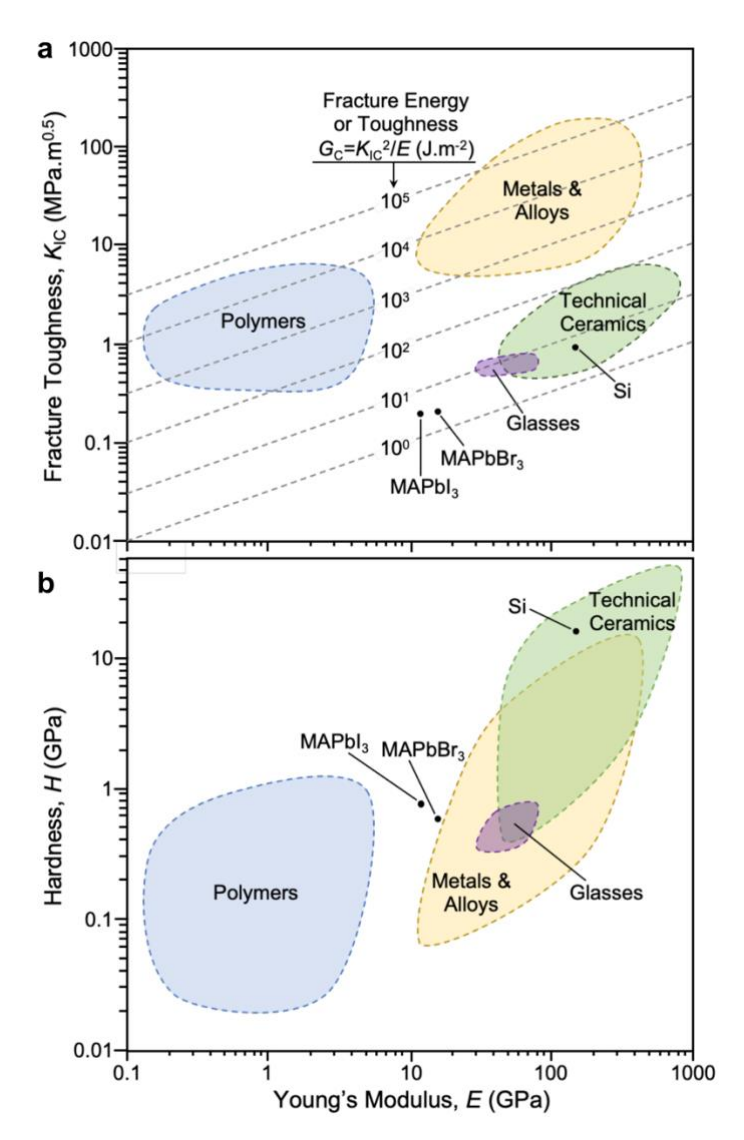


**Figure 14.** Materials-design 'Ashby' maps of regular classes of materials, with two single-crystal MHPs data from ref.<sup>[125]</sup> included: (a) Young's modulus (E) - fracture toughness ( $K_{\rm IC}$ ) and (b) E - Hardness (H). Dashed lines in (a) represent equal plane-stress toughness ( $G_{\rm C}$ ). Materials-design map adapted from ref.<sup>[127]</sup> and using typical properties of selected sets of materials.

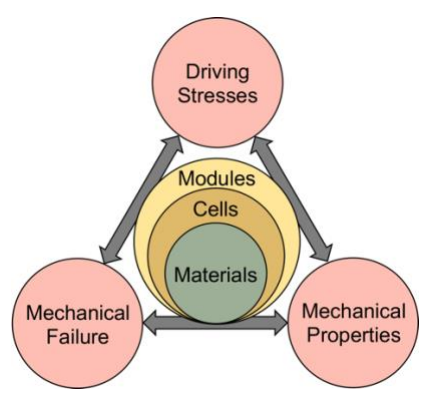


Figure 15. Complex interplay between the three essential elements that determines the mechanical

reliability of MHPs, PSCs, and PSMs.<sup>[83]</sup> Reproduced with permission.

### Outlook

Solar PVs are likely to play a major role in the decarbonized power sector of the future, and, therefore, there is always going to be a demand for low 'carbon-footprint' new PV technologies that are more efficient, reliable, and cost-effective. The burgeoning MHP-based PV technology offers great promise in that regard, but significant challenges lie ahead. It is likely that niche applications is where MHP-based PVs may find commercial success first, but TW-scale impact will need low-cost, science-based solutions to the following primary challenges. First, record PCEs of large-area PSMs for single-junction and tandem PVs need to approach close to those demonstrated in corresponding smaller-area PSCs. Second, single-junction PSMs need to have sufficient operational-stability and reliability to be certified for 20-25 years of useful life, and in tandem PVs, the PSMs need to be prime-reliant. Third, PSMs must be environmentally safe to manufacture and operate. Finally, PSMs must have a low 'carbon footprint,' and use only earth-abundant materials. The prize of widespread commercialization of the MHP-based PV technology, and the prospect of doing fascinating science along the way, make addressing these challenges a worthwhile endeavor.

# Acknowledgements

I thank the members of my research group, current (Z. Dai, M.C. Doyle, H.F. Garces, M. Layek, A. Ranka, I. Yang) and former (C.E. Athanasiou, M. Chen, Q. Dong, O.S. Game, J. Gong, M. Hu, H. Khassaf, T. Liu, A.R. Krause, C. Ramírez, H. Sternlicht, A.L. Vasiliev, Q. Wang, S.K. Yadavalli, Y. Zhang, Y. Zhou, and Y. Zong), and the vast network of collaborators, who have taught me so much about MHPs and PVs. Funding for this work was provided by National Science Foundation (Grant No. 2102210), Office of Naval Research (Grant No. N00014-20-1-2574), and Department of Energy (DOE) Office of Energy Efficiency and Renewable Energy under the Solar Energy Technology Office (Award No. DE-0009511). The views expressed in the article do not necessarily represent the views of the DOE or the U.S. Government. Finally, this article is dedicated to the PSC pioneers, and winners of the 50th Rank Prize (2022) for Optoelectronics, who opened up this fascinating new field: (in alphabetical order) Prof. Michael Grätzel, Dr. Akihiro Kojima, Dr. Michael Lee, Prof. Tsutomo Miyasaka, Prof. Nam-Gyu Park, Prof. Sang Il Seok, and

Prof. Henry Snaith.

# **Conflict of interest**

The corresponding author states that there is no conflict of interest.

### References

- [1] N. M. Haegel, P. Verlinden, M. Victoria, P. Altermatt, H. Atwater, T. Barnes, C. Breyer, C. Case, S. D. Wolf, C. Deline, M. Dharmrin, B. Dimmler, M. Gloeckler, J. C. Goldschmidt, B. Hallam, S. Haussener, B. Holder, U. Jaeger, A. Jaeger-Waldau, I. Kaizuka, H. Kikusato, B. Kroposki, S. Kurtz, K. Matsubara, S. Nowak, K. Ogimoto, C. Peter, I. M. Peters, S. Philipps, M. Powalla, U. Rau, T. Reindl, M. Roumpani, K. Sakurai, C. Schorn, P. Schossig, R. Schlatmann, R. Sinton, A. Slaoui, B. L. Smith, P. Schneidewind, B. J. Stanbery, M. Topic, W. Tumas, J. Vasi, M. Vetter, E. Weber, A. W. Weeber, A. Weidlich, D. Weiss, A. W. Bett, *Science* 2023, 380, 39.
- [2] A. K. Jena, A. Kulkarni, T. Miyasaka, *Chem. Rev.* **2019**, 119, 3026.
- [3] T. Miyasaka, *Perovskite Photovoltaics and Optoelectronics: From Fundamentals to Advanced Applications*, Wiley-VCH, Weinheim, Germany **2021**.
- [4] X. Luo, X. Lin, F. Gao, Y. Zhao, X. Li, L. Zhan, Z. Qiu, J. Wang, C. Chen, L. Meng, X. Gao, Y. Zhang, Z. Huang, R. Fan, H. Liu, Y. Chen, X. Ren, J. Tang, C.-H. Chen, D. Yang, Y. Tu, X. Liu, D. Liu, Q. Zhao, J. You, J. Fang, Y. Wu, H. Han, X. Zhang, D. Zhao, F. Huang, H. Zhou, Y. Yuan, Q. Chen, Z. Wang, S. Liu, R. Zhu, J. Nakazaki, Y. Li, L. Han, *Sci. China Chem.* **2022**, 65, 2369.
- [5] X. Tian, S. D. Stranks, F. You, *Nature Sustain.* **2021**, 4, 821.
- [6] NREL Best Research-Cell Efficiency Chart <a href="https://www.nrel.gov/pv/interactive-cell-efficiency.html">https://www.nrel.gov/pv/interactive-cell-efficiency.html</a> Accessed on June 10, 2023.
- [7] A. Kojima, K. Teshima, Y. Shirai, T. Miyasaka, J. Am. Chem. Soc. 2009, 131, 6050.
- [8] B. O'Regan, M. Grätzel, *Nature* **1991**, 353, 737.
- [9] H.-S. Kim, C.-R. Lee, J.-H. Im, K.-B. Lee, T. Moehl, A. Marchioro, S.-J. Moon, R. Humphrey-Baker, J.-H. Yum, J. E. Moser, M. Grätzel, N.-G. Park, *Sci. Rep.* **2012**, 2, 591.
- [10] I. Chung, B. Lee, J. He, R. P. H. Chang, M. Kanatzidis, *Nature* **2012**, 485, 486.

- [11] M. M. Lee, J. Teuscher, T. Miyasaka, T. N. Murakami, H. J. Snaith, *Science* 2012, 338, 643.
- [12] J. H. Heo, S. H. Im, J. H. Noh, T. N. Mandal, C.-S. Lim, J. A. Chang, Y. H. Lee, H.-J. Kim, A. Sarkar, M. K. Nazeeruddin, M. Grätzel, S. I. Seok, *Nature Photon.* **2013**, 7, 486.
- [13] P. Docampo, J. M. Ball, M. Darwich, G. E. Eperon, H. J. Snaith, *Nature Commun.* **2013**, 4, 2761.
- [14] G. E. Eperon, V. M. Burlakov, P. Docampo, A. Goriely, H. J. Snaith, *Adv. Funct. Mater.*2014, 24, 151.
- [15] N. J. Jeon, J. H. Noh, Y. C. Kim, W. S. Yang, S. Ryu, S. I. Seok, *Nature Mater.* 2014, 9, 897.
- [16] T. M. Brenner, D. A. Egger, L. Kronik, G. Hodes, D. Cahen, *Nature Rev. Mater.* 2016, 1, 15007.
- [17] D. Shi, V. Adinolfi, R. Comin, M. Yuan, E. Alarousu, A. Buin, Y. Chen, A. Hoogland, A. Rothenberger, K. Katsiev, Y. Losovyj, X. Zhang, P. A. Dowben, O. F. Mohammed, E. H. Sargent, O. M. Bakr, *Science* **2015**, 347, 519.
- [18] Q. Dong, Y. Fang, Y. Shao, P. Mulligan, J. Qiu, L. Cao, J. Huang, Science 2015, 347, 967.
- [19] J.-Y. Shao, D. Li, J. Shi, C. Ma, Y. Wang, X. Liu, X. Jiang, M. Hao, L. Zhang, C. Liu, Y. Jiang, Z. Wang, Y.-W. Zhong, S. Liu, Y. Mai, Y. Liu, Y. Zhao, Z. Ning, L. Wang, B. Xu, L. Meng, Z. Bian, Z. Ge, X. Zhan, J. You, Y. Li, Q. Meng, Sci. China Chem. 2023, 66, 10.
- [20] Y. Gao, K. Huang, C. Long, Y. Ding, J. Chang, D. Zhang, L. Etgar, M. Liu, J. Zhang, J. Yang, ACS Energy Lett. 2022, 7, 1412.
- [21] S. H. Reddy, F. D. Giacomo, A. DiCarlo, Adv. Energy Mater. 2022, 12, 2103534.
- [22] A. W. Y. Ho-Baillie, J. H. Zheng, M. A. Mahmud, F. J. Ma, D. R. McKenzie, M. A. Green, *Appl. Phys. Rev.* **2021**, 8, 041307.
- [23] S. D. Wolf, J. Holovsky, S.-J. Moon, P. Löper, B. Niesen, M. Ledinsky, F.-J. Haug, J.-H. Yum, C. Ballif, *J. Phys. Chem. Lett.* **2014**, 5, 1035.
- [24] W.-J. Yin, T. Shi, Y. Yan, Appl. Phys. Lett. **2014**, 104, 063903.
- [25] K. Miyata, D. Meggiolaro, M. T. Trinh, P. P. Joshi, E. Mosconi, S. C. Jones, F. de Angelis, X. Y. Zhu, *Science Adv.* **2017**, 3, e1701217.
- [26] H. Zhang, N.-G. Park, J. Phys.: Energy 2023, 5, 024002.

- [27] J. M. Frost, K. T. Butler, F. Brivio, C. H. Hendon, M. van Schilfgaarde, A. Walsh, *Nano Lett.* **2014**, 14, 2584.
- [28] Y. Kutes, L. Ye, Y. Zhou, S. Pang, B. D. Huey, N. P. Padture, *J. Phys. Chem. Lett.* **2014**, 5, 3335.
- [29] W. L. Zheng, X. C. Wang, X. Zhang, B. Chen, H. Suo, X. F. Xing, Y. Z. Wang, H. L. Wei, J. K. Chen, Y. Guo, F. Wang, *Adv. Mater.* 2023, 35, 21.
- [30] L. M. Pazos-Outon, M. Szumilo, R. Lamboll, J. M. Richter, M. Crespo-Quesada, M. Abdi-Jalebi, H. J. Beeson, M. Vrucinic, M. Alsari, H. J. Snaith, B. Ehrler, R. H. Friend, F. Deschler, *Science* 2016, 351, 1430.
- [31] W. Raja, M. DeBastiani, T. G. Allen, E. Aydin, A. Razzaq, U. Rehman, E. Ugur, A. Babayigit, A. S. Subbiah, F. H. Isikgor, S. DeWolf, *Nanophoton.* **2021**, 10, 2023.
- [32] B. Saparov, D. B. Mitzi, Chem. Rev. 2016, 116, 4558.
- [33] W. A. Dunlop-Shohl, Y. Zhou, N. P. Padture, D. B. Mitzi, Chem. Rev. 2019, 119, 3193.
- [34] G. Kieslich, S. Sun, A.K. Cheetham, *Chem. Sci.* **5**, 4712 (2014).
- [35] L. Mao, C. C. Stoumpos, M. G. Kanatzidis, J. Am. Chem. Soc. 2019, 141, 1171.
- [36] J. Avila, C. Momblona, P. P. Boix, M. Sessolo, H. J. Bolink, *Joule* **2017**, 1, 431.
- [37] Z. Saki, M. M. Byranvand, N. Taghavinia, M. Kedia, M. Saliba, *Energy Environ. Sci.* **2021**, 14, 5690.
- [38] D. K. Lee, N.-G. Park, *Solar RRL* **2022**, 6, 2100455.
- [39] J. Yan, T. J. Savenije, L. Mazzarella, O. Isabella, Sustain. Energy Fuels 2022, 6, 243.
- [40] F. Wang, Y. Han, D. Duan, C. Ge, H. Hu, G. Li, *Energy Rev.* **2022**, 1, 100010.
- [41] Y. Deng, Z. Zheng, Y. Bai, Q. Wang, J. Zhao, J. Huang, *Nature Energy* 2018, 3, 560.
- [42] Y. Deng, C. H. van Brackle, X. Dai, J. Zhao, B. Chen, J. Huang, *Science Adv.* **2019**, 5, eaax7537.
- [43] J. Troughton, M. J. Carnie, M. L. Davies, C. Charbonneau, E. H. Jewell, D. A. Worsley, T. M. Watson, *J. Mater. Chem. A* 2016, 4, 3471.
- [44] N. Rolston, W. J. Scheideler, A. C. Flick, J. P. Chen, H. Elmaraghi, A. Sleugh, O. Zhao, M. Woodhouse, R. H. Dauskardt, *Joule* **2020**, 4, 2675.
- [45] Y. Jiang, S. He, L. Qiu, Y. Zhao, Y. Qi, *Appl. Phys. Rev.* **2022**, 9, 021305.
- [46] Y. Zhou, O. S. Game, S. Pang, N. P. Padture, J. Phys. Chem. Lett. 2015, 6, 4827.

- [47] Y. Zhou, N. P. Padture, in *Perovskite Photovoltaics and Optoelectronics Fundamentals to Advanced Applications*, (Ed: T. Miyasaka), Wiley, New York, NY 2021.
- [48] S. K. Yadavalli, M. Hu, N. P. Padture, *Scripta Mater.* **2021**, 196, 113748.
- [49] J. Song, Y. Zhou, N. P. Padture, B. D. Huey, *Nature Commun.* **2020**, 11, 3308.
- [50] F. Ji, S. Pang, L. Zhang, Y. Zong, G. Cui, N. P. Padture, Y. Zhou, ACS Energy Lett. 2017, 2, 2727.
- [51] M. U. Rothmann, J. S. Kim, J. Borchert, K. B. Lohmann, C. M. O'Leary, A. A. Sheader, L. Clark, H. J. Snaith, M. B. Johnston, P. D. Nellist, L. M. Herz, *Science* 2020, 370, eabb5940.
- [52] Y. Zong, Y. Zhou, Y. Zhang, Z. Li, L. Zhang, M.-G. Ju, M. Chen, S. Pang, X. C. Zeng, N. P. Padture, CHEM 2018, 4, 1404.
- [53] T. Liu, Y. Zhou, Z. Li, L. Zhang, M.-G. Ju, D. Luo, Y. Yang, M. Yang, D. Kim, W. Yang, N.P.Padture, M. C. Beard, X. C. Zeng, K. Zhu, Q. Gong, R. Zhu, Adv. Energy Mater. 2018, 8, 1800232.
- [54] Y. Zong, Z. Zhou, M. Chen, N. P. Padture, Y. Zhou, Adv. Energy Mater. 2018, 8, 1800997.
- [55] M. Schroeder, *Fractals, Chaos and Power Laws*, W.H. Freeman & Co., New York, NY **1991**.
- [56] S. K. Yadavalli, Z. Dai, M. Hu, Q. Dong, W. Li, Y. Zhou, R. Zia, N. P. Padture, *Acta Mater.* **2020**, 193, 10.
- [57] Y. Zhou, L. M. Herz, A. K.-Y. Jen, M. Saliba, *Nature Energy* **2022**, 7, 794.
- [58] N. Giesbrecht, J. Schlipf, L. Oesinghaus, A. Binek, T. Bein, P. Müller-Buschbaum, P. Docampo, *ACS Energy Lett.* **2016**, 1, 150.
- [59] S. Y. Leblebici, L. Leppert, Y. Li, S. E. Reyes-Lillo, S. Wickenburg, E. Wong, J. Lee, M. Melli, D. Ziegler, D. K. Angell, D. F. Ogletree, P. D. Ashby, F. M. Toma, J. B. Neaton, I. D. Sharp, A. Weber-Bargioni, *Nature Energy* 2016, 1, 16093.
- [60] C. Ma, F. T. Eickemeyer, S.-H. Lee, D.-H. Kang, S. J. Kwon, M. Grätzel, N.-G. Park, *Science* **2023**, 379, 173.
- [61] L. N. Quan, M. Yuan, R. Comin, O. Voznyy, E. M. Beauregard, S. Hoogland, A. Buin, A. R. Kirmani, K. Zhao, A. Amassian, D. H. Kim, E. H. Sargent, J. Am. Chem. Soc. 2016, 138, 2649.
- [62] H. Tsai, W. Nie, J.-C. Blancon, C. C. Stoumpos, R. Asadpour, B. Harutyunyan, A. J. Neukirch, R. Verduzco, J. J. Crochet, S. Tretiak, L. Pedesseau, J. Even, M. A. Alam, G.

- Gupta, J. Lou, P. M. Ajayan, M. J. Bedzyk, M. G. Kanatzidis, A. D. Mohite, *Nature* **2016**, 536, 313.
- [63] A. Swarnkar, A. R. Marshall, E. M. Sanehira, B. D. Chernomordik, D. T. Moore, J. A. Christians, T. Chakrabarti, J. M. Luther, *Science* **2016**, 354, 92.
- [64] W. Chi, S. K. Banerjee, *Angew. Chem. Intl. Ed.* **2021**, 61, e202112412.
- [65] R. Chen, W. Zhang, X. Guan, H. Raza, S. Zhang, Y. Zhang, P. A. Troshin, S. A. Kuklin, Z. Liu, W. Chen, *Adv. Funct. Mater.* 2022, 32, 2200651.
- [66] L. Lin, T. W. Jones, T. C.-J. Yang, N. W. Duffy, J. Li, L. Zhao, B. Chi, X. Wang, G. J. Wilson, Adv. Funct. Mater. 2021, 31, 2008300.
- [67] Q. Jiang, X. W. Zhang, J. B. You, Small 2018, 14, 1801154.
- [68] S. Y. Park, K. Zhu, Adv. Mater. 2022, 34, 2110438.
- [69] P. Mahajan, B. Padha, S. Verma, V. Gupta, R. Datt, W. C. Tsoi, S. Satapathi, S. Arya, *J. Energy Chem.* **2022**, 68, 330.
- [70] A. Al-Ashouri, A. Magomedov, M. Roß, M. Jost, M. Talaikis, G. Chistiakova, T. Bertram, J. A. Marquez, E. Koehnen, E. Kasparavicius, S. Levcenco, L. Gil-Escrig, C. J. Hages, R. Schlatmann, B. Rech, T. Malinauskas, T. Unold, C. A. Kaufmann, L. Korte, G. Niaura, V. Getautis, S. Albrecht, *Energy Environ. Sci.* 2019, 12, 3356.
- [71] B. Yang, S. Peng, W. C. H. Choy, *EcoMat* **2021**, 3, e12127.
- [72] H. Kroemer, 51<sup>st</sup> Lindau Nobel Laureate Meeting, "Heterostructures for Everything?" <u>https://mediatheque.lindau-nobel.org/meetings/2001/programme/30466/2001-heterostructures-for-everything</u> Accessed June 10, **2023**.
- [73] P. Schulz, D. Cahen, A. Kahn, *Chem. Rev.* **2019**, 119, 3349.
- [74] Z. Guo, Z. Wu, Y. Chen, S. Wang, W. Huang, J. Mater. Chem. C 2022, 10, 13611.
- [75] F. H. Isikgor, S. Zhumagali, L. V. T. Merino, M. DeBastiani, I. McCulloch, S. DeWolf, *Nature Rev. Mater.* **2023**, 8, 89.
- [76] N. Rolston, B. L. Watson, C. D. Bailie, M. D. McGehee, J. P. Bastos, R. Gehlhaar, J.-E. Kim, D. Vak, A. T. Mallajosyula, G. Gupta, A. D. Mohite, R. H. Dauskardt, *Extrem. Mech. Lett.* 2016, 9, 353.
- [77] C. Ramirez, S. K. Yadavalli, H. F. Garces, Y. Zhou, N. P. Padture, *Scripta Mater.* **2018**, 150, 36.

- [78] N. Rolston, K. A. Bush, A. D. Printz, A. Gold-Parker, Y. Ding, M. F. Toney, M. D. McGehee, R. H. Dauskardt, Adv. Energy Mater. 2018, 8, 1802139.
- [79] M. Gutwald, N. Rolston, A. D. Printz, O. Zhao, H. Elmaraghi, Y. Ding, J. Zhang, R. H. Dauskardt, *Solar Energy Mater. Solar Cells* **2020**, 209, 110433.
- [80] Z. Dai, S. K. Yadavalli, M. Chen, A. Abbaspourtamijani, Y. Qi, N. P. Padture, *Science* **2021**, 372, 618.
- [81] Q. Tu, D. Kim, M. Shyikh, M. G. Kanatzidis, *Matter* **2021**, 4, 2765.
- [82] Z. Dai, S. Li, X. Liu, M. Chen, C. E. Athanasiou, B. W. Sheldon, H. Gao, P. Guo, N. P. Padture, *Adv. Mater.* **2022**, 34, 2205301.
- [83] Z. Dai, N. P. Padture, *Nature Energy*, in press, **2023**.
- [84] S. Y. Kim, S. J. Cho, S. E. Byeon, X. He, H. Y. Yoon, *Adv. Energy Mater.* **2020**, 10, 2002606.
- [85] F. Ali, C. Roldan-Carmona, M. Sohail, M. K. Nazeeruddin, *Adv. Energy Mater.* **2020**, 10, 2002989.
- [86] J. Park, J. Kim, H.-S. Yun, M. J. Paik, E. Noh, H. J. Mun, M. G. Kim, T. J. Shin, S. I. Seok, *Nature* 2023, 616, 724.
- [87] H. J. Snaith, A. Abate, J. M. Ball, G. F. Eperon, T. Leijtens, N. K. Noel, S. D. Stranks, J. T.-W. Wang, K. Wojciechowski, W. Zhang, *J. Phys. Chem. Lett.* **2014**, 5, 1511.
- [88] C. Wang, C. Xiao, Y. Yu, D. Zhao, R. A. Awni, C. R. Grice, K. Ghimire, I. Constantinou, W. Liao, A. J. Cimaroli, P. Liu, J. Chen, N. J. Podraza, C.-S. Jiang, M. M. Al-Jassim, X. Zhao, Y. Yan, *Adv. Energy Mater.* 2017, 7, 1700414.
- [89] K. O. Brinkmann, T. Becker, F. Zimmermann, C. Kreusel, T. Gahlmann, T. Haeger, T. Riedl, *Solar RRL* **2021**, 5, 2100371.
- [90] Z. Guo, A. K. Jena, G. M. Kim, T. Miyasaka, *Energy Environ. Sci.* **2022**, 15, 3171.
- [91] M. A. Green, E. D. Dunlop, G. Siefer, M. Yoshita, N. Kopidakis, K. Bothe, X. Hao, *Prog. Photovolt. Res. Appl.* **2023**, 31, 3.
- [92] Y. Rong, Y. Hu, A. Mei, H. Tran, M. I. Saidaminov, S. I. Seok, M. McGehee, E. H. Sargent,
   H. Han, *Science* 2018, 361, 1214.
- [93] S. P. Dunfield, L. Bliss, F. Zhang, J. M. Luther, K. Zhu, M. F. A. M. v. Hest, M. O. Reese, J. J. Berry, *Adv. Energy Mater.* 2020, 10, 1904054.

- [94] G. P. Nagabhushana, R. Shivaramaiah, A. Navrotsky, *Proc. Natl. Acad. Sci.* **2016**, 113, 7717.
- [95] M. Saliba, T. Matsui, J.-Y. Seo, K. Domanski, J.-P. Correa-Baena, M. K. Nazeeruddin, S. M. Zakeeruddin, W. Tress, A. Abate, A. Hagfeldt, M. Graetzel, *Energy Environ. Sci.* 2016, 9, 1989.
- [96] Z. Li, M. Yang, J.-S. Park, S.-H. Wei, J. J. Berry, K. Zhu, *Chem. Mater.* **2016**, 28, 284.
- [97] W. Travis, E. N. K. Glover, H. Bronstein, D. O. Scanlon, R. G. Palgrave, *Chem. Sci.* **2016**, 7, 4548.
- [98] H. Zai, Y. Ma, Q. Chen, H. Zhou, *J. Energy Chem.* **2021**, 63, 528.
- [99] Q. Wang, B. Chen, Y. Liu, Y. Deng, Y. Bai, Q. Dong, J. Huang, *Energy Environ. Sci.* **2017**, 10, 516.
- [100] E. T. Hoke, D. J. Slotcavage, E. R. Dohner, A. R. Bowring, H. I. Karunadasa, M. D. McGhee, *Chem. Sci.* **2015**, 6, 613.
- [101] K. Suchan, J. Just, P. Beblo, C. Rehermann, A. Merdasa, R. Mainz, I. G. Scheblykin, E. Ungar, *Adv. Funct. Mater.* **2023**, 33, 2206047.
- [102] M. Saliba, M. Stolterfoht, C. M. Wolff, D. Neher, A. Abate, *Joule* **2018**, 2, 1019.
- [103] S. Bae, S. Kim, S.-W. Lee, K. J. Cho, S. Park, S. Lee, Y. Kang, H.-S. Lee, D. Kim, J. Phys. Chem. Lett. 2016, 7, 3091.
- [104] M. V. Khenkin, E. A. Katz, A. Abate, G. Bardizza, J. J. Berry, C. Brabec, F. Brunetti, V. Bulović, Q. Burlingame, A. D. Carlo, R. Cheacharoen, Y.-B. Cheng, A. Colsmann, S. Cros, K. Domanski, M. Dusza, C. J. Fell, S. R. Forrest, Y. Galagan, D. D. Girolamo, M. Grätzel, A. Hagfeldt, E. v. Hauff, H. Hoppe, J. Kettle, H. Kob er, M. S. Leite, S. Liu, Y.-L. Loo, J. M. Luther, C.-Q. Ma, M. Madsen, M. Manceau, M. Matheron, M. McGehee, R. Meitzner, M. K. Nazeeruddin, A. F. Nogueira, Ç. Odabaşı, A. Osherov, N.-G. Park, M. O. Reese, F. D. Rossi, M. Saliba, U. S. Schubert, H. J. Snaith, S. D. Stranks, W. Tress, P. A. Troshin, V. Turkovic, S. Veenstra, I. Visoly-Fisher, A. Walsh, T. Watson, H. Xie, R. Yıldırım, S. M. Zakeeruddin, K. Zhu, M. Lira-Cantu, *Nature Energy* 2020, 5, 35.
- [105] K. Domanski, E. A. Alharbi, A. Hagfeldt, M. Grätzel, W. Tress, *Nature Energy* **2018**, 3, 61.
- [106] Y. Miyazawa, M. Ikegami, H.-W. Chen, Y. Ohshima, M. Imaizumi, K. Hirose, T. Miyasaka, *iScience* **2018**, 2, 148.

- [107] W. Delmas, S. Erickson, J. Arteaga, M. Woodall, M. Scheibner, T. S. Krause, K. Crowley, K. T. VanSant, J. M. Luther, J. N. Williams, J. McNatt, T. J. Peshek, L. McMillon-Brown, S. Ghosh, *Adv. Energy Mater.* 2023, 13, 2203920.
- [108] S. Sidhik, Y. F. Wang, M. D. Siena, R. Asadpour, A. J. Torma, T. Terlier, K. Ho, W. B. Li, A. B. Puthirath, X. T. Shuai, A. Agrawal, B. Traore, M. Jones, R. Giridharagopal, P. M. Ajayan, J. Strzalka, D. S. Ginger, C. Katan, M. A. Alam, J. Even, M. G. Kanatzidis, A. D. Mohite, *Science* 2022, 377, 1425.
- [109] D. H. Kim, J. B. Whitaker, Z. Li, M. F. A. M. v. Hest, K. Zhu, *Joule* **2018**, 2, 1437.
- [110] Y. Cheng, Y. Peng, A. K.-Y. Jen, K.-L. Yip, Solar RRL 2022, 6, 2100545.
- [111] M. Kim, J. Jeong, H. Lu, T. K. Lee, F. T. Eickemeyer, Y. Liu, I. W. Choi, S. J. Choi, Y. Jo, H.-B. Kim, S.-I. Mo, Y.-K. Kim, H. Lee, N. G. An, S. Cho, W. R. Tress, S. M. Zakeeruddin, A. Hagfeldt, J. Y. Kim, M. Grätzel, D. S. Kim, *Science* 2022, 375, 302.
- [112] NREL Best Modules Efficiency Chart, <a href="https://www.nrel.gov/pv/module-efficiency.html">https://www.nrel.gov/pv/module-efficiency.html</a>
  Accessed on June 10, 2023.
- [113] S. Ma, G. Yuan, Y. Zhang, N. Yang, Y. Li, Q. Chen, Energy Environ. Sci. 2022, 15, 13.
- [114] Y. Wang, I. Ahmad, T. Leung, J. Lin, W. Chen, F. Liu, A. M. C. Ng, Y. Zhang, A. B. Djurišić, *ACS Mater. Au* **2022**, 2, 215.
- [115] A. Babayigit, A. Ethirajan, M. Muller, B. Connings, Nature Mater. 2016, 15, 247.
- [116] N. Moody, S. Sesena, D. W. deQuilettes, B. D. Dou, R. Swartwout, J. T.Buchman, A. Johnson, U. Eze, R. Brenes, M. Johnston, C. L.Haynes, V. Bulović, M. G.Bawendi, *Joule* 2020, 4, 970.
- [117] B. Hailegnaw, S. Kirrmayer, E. Edri, G. Hodes, D. Cahen, *J. Phys. Chem. Lett.* **2015**, 6, 1543.
- [118] M.-G. Ju, M. Chen, Y. Zhou, J. Dai, L. Ma, N. P. Padture, X. C. Zeng, *Joule* **2018**, 2, 1231.
- [119] M. Chen, M.-G. Ju, A. D. Carl, Y. Zong, R. L. Grimm, J. Gu, X. C. Zeng, Y. Zhou, N. P. Padture, *Joule* 2018, 2, 558.
- [120] W. Ke, M. G. Kanatzidis, *Nature Commun.* **2019**, 10, 965.
- [121] J. J. Berry, M. D. Irwin, APL Energy 2023, 1, 010902.
- [122] H. Zhang, J.-W. Lee, G. Nasti, R. Handy, A. Abate, M. Grätzel, N.-G. Park, *Nature* **2023**, 617, 687.
- [123] M. Dailey, Y. Li, A. D. Printz, ACS Omega 2021, 6, 30214.

- [124] D. Liu, D. Luo, A. N. Iqbal, K. W. P. Orr, T. A. S. Doherty, Z.-H. Lu, S. D. Stranks, W. Zhang, *Nature Mater.* 2021, 20, 1337.
- [125] Z. Dai, M. C. Doyle, X. Liu, M. Hu, Q. Wang, C. E. Athanasiou, Y. Liu, S. Z. Liu, B. W. Sheldon, H. Gao, N. P. Padture, *Scripta Mater.* **2023**, 223, 115064.
- [126] S. K. Yadavalli, Z. Dai, H. Zhou, Y. Zhou, N. P. Padture, *Acta Mater.* **2020**, 187, 112.
- [127] M. Ashby, H. Shercliff and D. Cebon, *Materials: Engineering, Science, Processing and Design*, Butterworth-Heinemann, Oxford, UK **2007**.